Revised for J. Geophys Res. 16 March 1998

Optical backscattering by calcifying algae--Separating the contribution by particulate inorganic and organic carbon fractions

William M. Balch, David T. Drapeau, Terry L. Cucci, and Robert D. Vaillancourt
Bigelow Laboratory for Ocean Sciences
P.O. Box 475
West Boothbay Harbor, ME 04575 U.S.A.

Katherine A. Kilpatrick
Division of Meterology and Physical Oceanography
Rosenstiel School for Marine and Atmospheric Science
University of Miami
4600 Rickenbacker Causeway
Miami, FL 33149-1098 U.S.A.

Jennifer J. Fritz
Smithsonian Environmental Research Center
P. O. Box 28
Edgewater, MD 21037 U.S.A.

GAP Key words: Calcium carbonate, coccolithophores, coccoliths, backscattering
Running head: Optical backscattering by calcifying algae

Abstract

Light scattering properties of biogenic $CaCO_3$ particles (particulate inorganic carbon; PIC) were determined on cultured calcifying algae and field-derived $CaCO_3$ particles. The particles were separated from particulate organic carbon (POC) with a flow cytometer, volume scattering functions were measured with a laser light scattering photometer, and particle composition was measured using atomic absorption spectrometry. Small calcite coccoliths were best sorted by gating on the ratio of horizontally-polarized forward light scattering and vertically-polarized forward light scattering; plated coccolithophores could be sorted by gating on side scattering and forward angle light scattering. Normalized volume scattering functions for the culture-derived calcite particles varied by a factor of two for the different species. Backscattering cross-sections (m^2 $particle^{-1}$) for calcite particles varied by about 3500% and were generally a function of size. Backscattering efficiencies were ~2-4X higher for cells with $CaCO_3$ than without it. $CaCO_3$-specific backscattering showed much less variability across various species; the calcite-specific backscattering coefficient varied by only ~38%, for both cultured coccolithophores and field-derived $CaCO_3$ particles. Organic carbon-specific backscattering of "naked" coccolithophores was highly consistant within all coccolithophores used in our experiments, as well as with previous literature values. Our results demonstrate that both POC and PIC can be optically estimated, the former by measuring backscattering of de-calcified phytoplankton as well as their size distribution, and the latter is proportional to acid-labile backscattering. These results show the feasibility of a rapid optical technique for measuring two biogeochemically important carbon fractions in the sea.

1. Introduction

1.1 Production of calcium carbonate and organic carbon in the sea

Biogenic sediments make up about half the sediments that accumulate on the sea floor. Of this amount, most of the biogenic sediments consist of calcite or opal, while organic sedimentation contributes between a few tenths of a percent, up to 5% in highly productive areas. Thus, the majority of biogenic carbon deposition is as particulate inorganic production (PIC), such that calcium carbonate sediments represent 20-30% of all marine sediments [Broecker and Peng, 1982; Siebold and Berger, 1982].

The current global calcium carbonate production rate is about 5 Gtons $CaCO_3$ y^{-1} (=0.6 Gtons C as $CaCO_3$ y^{-1}) with half accumulating in the deep sea and the remainder being deposited on shallow reefs, and banks [Milliman, 1993]. Annual PIC production represents only about 1-3% of the global production of particulate organic carbon (POC; ~20-50 Gtons C y^{-1}) [Steemann Nielsen, 1954; Fleming, 1957; Koblents-Mishke et al., 1970; Ryther, 1969; Leith and Whittaker, 1975; Platt and Subba Rao, 1975; Berger, 1989; and Longhurst et al., 1995] but due to extremely efficient remineralization of organic tissue by bacteria and higher organisms, calcium carbonate dominates carbon burial in many regions. Predictions of $CaCO_3$ sedimentation have varied widely, however.

Milliman [1993] suggested that 60% of calcium carbonate accumulates in sediments. Westbroek et al.[1993] argued that global calcium carbonate production was ~1 Gton C y^{-1}, with only about 17% reaching the "geological archive". Broecker and Peng [1982] claimed that the average production rate of $CaCO_3$ is about 0.4 Gtons C y^{-1} with about 14% reaching the sediments. As Milliman [1993] pointed out, the reason for the factor of two difference in these production and accumulation rates was that many different data sets were used, with a wide range of assumptions. To put these numbers into perspective, the stoichiometry of calcification is such that with global calcification of 0.6 Gtons C y^{-1}(=50 Gmol C y^{-1}), about the same moles of CO_2 would be produced annually. This represents ~1/8 of annual fossil fuel CO_2 production, and is equal in magnitude to CO_2 production associated with timber cutting and agricultural tilling of soils [Broecker and Peng, 1982].

1.2 Variability in optical properties associated with PIC and POC

In order to estimate PIC and POC standing stocks via satellite remote sensing of ocean color, one must define their inherent optical properties, and relate these to the water-leaving radiances or reflectances. Of all the inherent optical properties measured in the sea, most is known about the variability of beam attenuation (c), the sum of absorption (a) and scattering (b). Beam attenuation is strongly related to the suspended particulate load [Kiefer and Austin, 1974; Spinrad and Zaneveld, 1982; Gordon and Morel, 1983]. It is generally believed that the majority of particulate beam attenuation is from small particles (<20μm)[Pak et al., 1988; Richardson et al., 1993]. Flow cytometry has been essential to understand variability in beam attenuation of these small particles, as well as to detect changes in cellular scattering on time scales of hours to days [Ackleson and Spinrad, 1988; Olson et al., 1990] .

Particle beam attenuation often varies diurnally [Siegel et al., 1989; Abbott et al., 1990; Walsh, 1990; Dickey et al, 1991; Cullen et al., 1992; Gardner et al., 1993; Gardner et al, 1995]. Stramski and Reynolds [1993] documented diurnal changes of 80% in attenuation and scattering cross-sections of a cultured diatom, mainly due to changes in cell size and refractive index. Diurnal cycling of beam attenuation has been attributed to several factors: changes in cellular optical properties, primary production and grazing, and diurnal changes to the mixed layer depth, with associated dilution of particles. Stramski and Reynolds [1993] showed that this variability could be reduced by 3X when the attenuation cross-section was normalized to cellular organic carbon. They concluded that the diurnal cycle of beam attenuation was more a function of the molar quantity of organic carbon than the particle concentration.

There has also been some question as to which particles, organic or inorganic, are most responsible for the beam attenuation in the sea. Kitchen and Zaneveld [1990] demonstrated that beam attenuation was poorly correlated to phytoplankton chlorophyll *a* in case I waters of the Northeastern Pacific Gyre near the Sub-Tropical Front. Their results were similar to Brown and Gordon [1973] and Zaneveld et al. [1974] in which most of the particles (70%) had a low refractive index, but 90% of the scattering was due to particles with high index of refraction (e.g. "hard" biogenic particles or lithogenic

particles). Two points need to be emphasized. First, bio-optical studies have focused on the impact of phytoplankton chlorophyll on absorption, scattering, and attenuation, but it has been clearly demonstrated that phytoplankton chlorophyll can account for much of the absorption, but only a fraction of the total scattering, backscattering and attenuation. Second, particle size, unlike chlorophyll, is a good predictor of beam attenuation, which suggests that the optical properties of autotrophic and heterotrophic organisms, plus their associated debris, and any minerogenic particles are important to total attenuation and scattering [Kitchen and Zaneveld, 1990; Morel and Ahn, 1991].

In terms of modeling remote sensing reflectance, absorption and backscattering are the critical inherent optical properties [Gordon et al., 1988]. While absorption can be well modeled by chlorophyll concentration, particulate backscattering in Case II waters is the sum of backscattering from water (b_{bwater}), autotrophes (b_{bauto}), heterotrophes ($b_{bhetero}$), organic detritus (b_{bdet}), and inorganic sedimentary components such as calcium carbonate (b_{bcalc}), clays (b_{bclay}), and opal(b_{bopal}). This can be summarized in equation 1:

$$b_{btot} = b_{bwater} + b_{bauto} + b_{bhetero} + b_{bdet} + b_{bcalc} + b_{bclay} + b_{bopal} \quad (1)$$

This can be simplified by pooling organic, biogenic PIC and lithogenic backscattering (such as from opal):

$$b_{btot} = b_{bwater} + b_{bPOC} + b_{bPIC} + b_{blithogenic} \quad (2)$$

In regions where non-carbonate, lithogenic backscattering is low, then particulate backscattering can be modeled as the sum of b_{bPIC} and b_{bPOC}. In most Case I waters examined by us, b_{bPIC} is usually at least ~10% of total particulate backscattering [e.g. Balch et al., 1996a and b] due to the ubiquitous distribution of coccoliths, even in nonbloom waters. At present, it is not known how important opal backscattering is to total backscattering in diatom-dominated Case I waters.

In this paper, we focus on the backscattering properties of calcifying algae. We used a flow cytometer to separate calcium carbonate particles (e.g. detached coccoliths) from the organic carbon fractions, and then measured the scattering properties of each sort using a light scattering photometer. Results from these studies will be important for developing an algorithm for remote-sensing of calcium carbonate and particulate organic carbon in the sea.

2. Methods

2.1 Growth of algal cultures

Cultures for all experiments were from the Center for the Culture of Marine Phytoplankton (CCMP; Bigelow Laboratory for Ocean Sciences, W. Boothbay Harbor, ME 04575) and grown in 1 liter flasks. They were transferred weekly into autoclaved K media [Keller et al., 1987] and were harvested in logarithmic growth. They were grown in batch cultures at 66.5 μEin m^{-2} s^{-1} PAR on a 14:10 h light:dark cycle. A summary of the algal clones and growth conditions is given in Table 1. Cell and detached coccolith counts were performed daily for 1-2 weeks prior to each experiment. Culture optical properties were always examined during early to mid- logarithmic growth, unless otherwise noted.

2.2 Experimental design

There were four types of experimental design used in the this optical study; all involved particle sorting with a flow cytometer, light scattering measurements of the sorts, acidification of a subsample to verify $CaCO_3$ dissolution, and microscope particle enumeration. All but one experimental design involved measurements of the $CaCO_3$ concentration. All experimental details are outlined in Table 2.

The EPICS-V flow cytometer,with multiparameter data acquisition was used to sort individual particles. Details on the instrument and its calibration can be found in Balch et al. [1993]. Coccoliths or coccolith-covered cells were run through the flow cytometer while gating on various optical properties. Two or three of the following sorting criteria were typically used: cell-specific forward angle light scattering (range=1.5°-19°, hereafter called FALS), 90° volume scattering (range=73°-107°, hereafter called 90°VS), chlorophyll fluorescence, horizontally- or vertically-polarized forward angle light scattering. Identification of calcite coccoliths was always verified by 1) sorting a specific number of detached coccoliths onto a microscope slide, and verifying the count microscopically and 2) verifying complete disappearance of the calcite particles upon bubbling with CO_2 gas for 30s [Paasche, 1962] or acidifying with glacial acetic acid to a final concentration of 1.33×10^{-2}% by volume. Once gating criteria were defined, calcite particles were sorted into ultraclean scintillation vials containing 5

ml of 0.2μm filtered seawater. Typically, serial additions of 10^4 plated coccolithophore cells or 10^5 detached coccoliths were sufficient for subsequent optical measurements.

Volume scattering is defined by Kirk [1994] as "the radiant intensity in a given direction from a volume element, dV, illuminated by a parallel beam of light, per unit of irradiance on the cross-section of the the volume, and per unit volume". Volume scattering (β_γ) for 436 nm, 546 nm or 632.8 light was measured on each sort (methods in Table 2). Then $CaCO_3$ in a subsample was dissolved to verify disappearance of the volume scattering. Photometer cuvettes were stirred with a small magnetic stir-bar to keep heavily-plated species from sinking during each measurement; this was particularly important for *Pleurochrysis* sp. and *Thoracosphaera* sp. Most particle-specific backscattering coefficients were measured at 632.8nm wavelength, with the exception of *E. huxleyi*, *Thoracosphaera* sp., and *Pleurochrysis* sp., in which all 3 wavelengths were measured.

The technique of Gordon [1976] was used to convert volume scattering functions to backscattering coefficients (b_b, that fraction of light scattered in the backwards direction per unit thickness; See Table 3 for list of symbols). Essentially, the volume scattering function (hereafter called VSF) was estimated as described in Table 2, and integrated in the backwards direction to calculate the backscattering coefficient. The difference between total and acidified backscattering was considered "acid-labile backscattering" (b_b'), which has been well calibrated to suspended calcite concentration [Balch et al., 1996b]. Linearity between numbers of particles and 90°VS was checked for each species to insure that multiple scattering was not occurring. As a cross check of the measurements made on particle sorts, b_b and b_b' were measured on bulk cultures (containing much more calcite), samples were filtered, rinsed with borate buffer (pH=9), frozen, and the $CaCO_3$ concentration measured (according to Table 2).

Several experiments involved sorting $CaCO_3$ particles based on their birefringence (technique described by Olson et al., 1989). Calcite rotates the plane of linearly polarized light by 90°. Moreover, it is well known that coccolith birefringence patterns are unique, thus aiding in species identification [Moshkovitz, 1989]. For these experiments, a "Quad" forward-angle detector was used in the Epics V flow cytometer. Two polarizing filters were placed over the two forward-angle

collectors of the Epics V flow cytometer, and oriented such that one accepted vertically-polarized forward angle light scattering (VFALS, same polarization orientation as the incident laser) while the second accepted horizontally-polarized forward angle light scattering (HFALS). To speed up the sorting of detached coccoliths, calcite particles were passed through 3μm nuclepore filters (except *Thoracosphaera* which was prescreened using 35μm Nitex mesh.).

In several experiments, we measured volume scattering of coccoliths from the Arabian Sea, and waters overlying the Dry Tortugas coral reef (Florida shelf waters). Samples were preserved with 5%, borate-buffered Formalin, and stored in refrigerated brown glass bottles until analysis. To have sufficient concentrations of field-derived coccoliths to sort in the flow cytometer, samples from various depths and stations were combined (400 ml total volume), and filter-concentrated onto 0.2μm pore-size nuclepore filters (2 ml final volume). While this mixing obviously blurred the exact sample location and depth, it provided a larger diversity of naturally-occuring coccoliths for optical analysis. Locations of the pooled samples are given in Table 4. Concentrates were filtered through 53μm Nitex mesh, to eliminate large aggregates, then vortexed with the original filter, to suspend the coccoliths. Each sample was then run through the Epics flow cytometer, gating on particle-specific VFALS and HFALS to discriminate coccoliths. Sorts were examined under the microscope, and calcite particles were subjected to 0.013% glacial acetic acid to verify complete dissolution.

3. Results

3.1 General Observations on Experimental Design

Flow cytometer counts were typically within 1% accuracy, when calculated at the beginning of a sort, but over longer sorts, numbers of sorted particles were over-estimated by ~15% compared to microscope counts of the same sample. This was due to drift in the amplifier noise at high gain settings, which changed over the course of a multi-hour sort.. Thus, in calculating particle specific backscattering, flow cytometer-based b_b^* values were corrected to b_b^* values based on microscope coccolith counts ($b_b^*{}_{CC}$) using the following equation:

$$b_b^*{}_{CC} = 0.858 * b_b^*{}_{FCM} + 1.73 \times 10^{-13} \quad (3)$$

($r^2 = 0.76$; n= 27)

Gating on FALS and 90°VS volume scattering was adequate for sorting plated coccolithophores (corrected counts were good to <1% compared to microscope counts; n=100), but was inefficient for sorting detached coccoliths. Sorts were still pure for the latter, they simply took longer to perform. For example, FALS and 90°VS of*Syracosphaera elongata* coccoliths overlapped with non-calcite particles, such that only ~30% of the population within the gate consisted of acid-labile coccoliths. This meant narrowing the gates to insure low overlap and pure sorts which lowered the sorting rate such that much longer sorting times were required. Addition of HFALS/VFALS ratios provided striking resolution of detached coccoliths from non-calcite particles. This was observed yet again when running field samples. Corrected counts were good to <1% when compared to microscope counts (n=100).

Scanning electron micrographs of the calcifying algal species are shown in Fig. 1. While coccospheres and calcite thecae were generally spherical, the cells ranged from 5.5-18 μm in diameter and the detached coccoliths/empty theceae varied from 1.6-11μm in diameter. Using autofluorescence, the flow cytometer could discriminate between coccospheres or thecae containing living cells, and empty coccospheres/thecae.

3.2 Normalized Volume Scattering Function and Particle-specific Backscattering Coefficients

Normalized volume scattering functions (NVSF's) of the various calcifying algae showed a factor of ~2 variance in $\tilde{\beta}$ in the forward and backwards directions (Fig. 2). *Thoracosphaera* had the steepest slope of the NVSF in the backwards direction.

Major differences in particle-specific b_b^* values were observed between plated cells versus detached coccoliths (Fig3; Table 5) and amongst the different species of plated cells (Fig. 4). Plots of b_b versus particle concentration *for individual species* were highly linear and the slope for pure biogenic calcite particles with no organic matter varied by 30-40X across the various species (Fig. 4; Table 5). When all species were pooled, however, there was no significant relationship between b_b and calcite particle concentration. Particle-specific scattering coefficients for plated cells were higher

than for detached coccoliths (Table 5) and the average values (i.e. slope of b_b versus concentration plots) showed higher variance for cells than for coccoliths.

To check for closure, sorts of naked, plated, and empty coccospheres were recombined, and the observed backscattering was compared with the predicted backscattering based on their respective particle-specific backscattering coefficients. We also enumerated naked, plated, or empty coccospheres in cultures, summed their respective particle-specific backscattering, and compared this with observed total backscattering. Equation 4 was used to predict backscattering, where the backscattering of the jth component was the product of its particle-specific backscattering coefficient (bb^*_j) and concentration (c_j).

$$b_{bpred} = \sum_{j=1}^{i} bb^*_j \times c_j$$

$$= (bb^*_{\text{pl cells}} \times c_{\text{pl cells}}) + (bb^*_{\text{n cells}} \times c_{\text{n cells}}) + (bb^*_{\text{coccoliths}} \times c_{\text{coccoliths}}) \quad (4)$$

Subscripts "pl cells", "n cells", "coccoliths" signify plated cells, naked cells, and detached coccoliths respectively. Results for the least squares fit of predicted vs. observed b_b showed a slope of only 0.34 (std err=0.13; n=27) and intercept of 4.2×10^{-3} (std err = 1.4×10^{-3}). The results were statistically significant but with low correlation (r^2 =0.23; F statistic=7.13 ; P<0.001). Observed b_b's were less than those predicted from equation 2, ~3/4 of the time (Fig. 5). The largest outlier was from unsorted *Pleurochrysis* sp..

Coccolith-specific backscattering by *E. huxleyi* was relatively constant over the different clones, and considerably less for naked than plated cells. Typically, heavily plated cells had a b_b* 5X larger than a naked cells, and naked cells had b_b* values about the same as detached coccoliths. *Cricosphaera* coccoliths had particle-specific backscattering similar to *E. huxleyi* coccoliths. Interestingly, *Thoracosphaera* sp. had high backscattering per cell, and plated cells produced backscattering which was only 1.4X that of naked cells. This meant that closure was not achieved--

backscattering of thecate cells ($1.1x10^{-11}$ m^2 $particle^{-1}$) was less than the sum of backscattering by empty thecae plus naked cells ($1.64x10^{-11}$ m^2 $particle^{-1}$; Table 5). There were a few cases with *Pleurochrysis* sp., where the same was observed (data not shown).

This was also seen in the backscattering efficiency (Q_{bb}) of the various clones (calculated as the backscattering cross section divided by the geometric cross section). Comparison of the plated and naked cell efficiency showed that plated *E.huxleyi*, *Syracosphaera*, and *Cricosphaera* were 2-3.5X more efficient at backscattering light than naked cells but *Thoracosphaera* and *Pleurochrysis* sp. actually backscattered more light per particle when they were naked (Fig 6).

Field-derived calcite particles showed particle-specific backscattering comparable to *Pleurochrysis* sp. and *Thoracosphaera* sp. cells (Fig. 3; Table 5). Only one sample (from stations 14-17 of the Arabian Sea Process cruise 4) had calcite particles with backscattering cross-sections approaching the average value for detached coccoliths of *E. huxleyi* (3.61×10^{-13} m^2 $particle^{-1}$; std dev. = 1.07×10^{-13} m^2 $particle^{-1}$; n=9). The rest of the sorted particles had b_b^* values 2-22X this value. It should be noted that, prior to performing these experiments, we checked two preservation techniques to see how preservation affected attachment and dissolution of coccoliths. Stationary-phase *E. huxleyi* (clone 88E) cells were preserved in both buffered Formalin and buffered Lugols iodine, and examined weekly for 30d, then monthly thereafter, for ~1/2 year. Coccoliths remained attached to coccolithophores in buffered Formalin, while significant numbers detached in buffered Lugols.

3.3 Calcite-specific Backscattering Coefficients

Backscattering coefficients of 6 calcifying algal species, as well as field-derived calcite particles, were normalized to the concentration of suspended calcite ($b_b^*{}_{Ca}$; m^2 $(mol\ Ca)^{-1}$) to see whether the the values of $b_b^*{}_{Ca}$ were less variable than $b_b^*{}_{partic}$. Results are shown in Fig. 7 and Table 5. The least squares fit line (at 632nm; forced through zero; standard errors given in square brackets) was:

$$b_{b\,Ca}[0.0042] = 6.95\ [0.492] \times C_{CaCO_3}$$

where C_{CaCO_3} designated the molar concentration of calcium carbonate (r^2=0.57; F=34.1; Degrees of freedom=26; residual sums of squares=$4.69x10^{-4}$; coefficient of variation of slope in Fig. 7=38%;

this varied slightly depending on whether or not the regression intercept was driven through zero). We observed that calcite-specific backscattering coefficients were higher when calculated on pure coccolith suspensions, instead of mixtures of plated cells and detached coccoliths, or mixtures of coccoliths, plated cells, and other noncalcifying species of phytoplankton. For example, pure sorts of *E. huxleyi* coccoliths had a $b_b{}^*_{Ca\ 632nm}$ of ~28 m^2 (mol Ca)$^{-1}$. Coccolith "filtrates" of the same species (which could have had contamination from cell fragments) gave values of $b_b{}^*_{Ca\ 632nm}$ = 7-15 m^2 (mol Ca)$^{-1}$. A mixture of E. huxleyi clone 88E plated cells and coccoliths had a $b_b{}^*_{Ca\ 632nm}$ of 4.22 m^2(mol Ca)$^{-1}$. In a North Atlantic coccolithophore bloom with plated cells, detached coccoliths, naked cells plus other phytoplankton species, showed $b_b{}^*_{Ca}$ = 2.11 and 1.63 m^2 (mol Ca)$^{-1}$ at 436 and 546nm, respectively (wavelength dependence of $\lambda^{-1.128}$). Correcting for wavelength would give $b_b{}^*_{Ca\ 632nm}$ = 1.39 m^2 (mol Ca)$^{-1}$, quite close to the acid-labile $b_b{}^*_{Ca}$ measured on a culture of *E. huxleyi* clone 89E (1.35 m^2 (mol Ca)$^{-1}$; Table 5).

Flow cytometer plots of chlorophyll fluorescence vs. 90°VS (plated cells; Fig. 8), or HFALS vs VFALS (detached coccoliths and or plated cells; Figs. 9 and 10) revealed changes in plated cell or coccolith scattering properties after dissolution of calcite coccoliths or thecae. Results for plated cells showed roughly the same chlorophyll fluorescence as acidified cells, but calcite dissolution significantly reduced 90°VS (Fig. 8). Acidification of *Thoracosphaera* cells actually increased chlorophyll fluorescence for the smaller cells but decreased it for the larger cells. Dissolution of calcite thecae had little impact on the 90°VS of *Thoracosphaera.* Untreated *E. huxleyi* showed two populations, confirmed microscopically to be heavily and lightly plated cells.

Cell autofluorescence was useful for sorting living coccolithophore cells, but it was more difficult (but still feasible) for sorting coccoliths since the latter were not autofluorescent. However, gating on HFALS and VFALS proved to be much more effective for isolating calcite particles (Fig. 9). Pre-filtering insured cells were absent from the medium prior to sorting, which made coccolith sorting more efficient (although smaller cell debris still was present and had to be sorted away with the flow cytometer). Microscopic examination of the sorts revealed that the particles were indeed coccoliths, further proven by their complete disappearance upon acidification. *E. huxleyi* (clone 89E) coccoliths

showed greater variability in VFALS than in HFALS. *E. huxleyi* (clone #1516) coccoliths had HFALS and VFALS remarkably similar to clone 89E of the same species. Acidification of the *E. huxleyi* clone #1516 culture completely dissolved the coccoliths and dropped the cellular VFALS into the range of the plot, as cells lost their covering of coccoliths. The HFALS vs. VFALS plot for *Cricosphaera* looked almost the same as for *E. huxleyi*. While empty *Thoracosphaera* thecae also almost completely disappeared upon acidification, they showed more variability in the HFALS than VFALS.

A major difference between the experiments with cultured coccolithophores and field-derived calcite particles was that the latter involved preservation with buffered Formalin. Examination of preserved *E. huxleyi* showed no significant loss of detached or attached coccoliths or plated cells (i.e. no dissolution) over 6 months of storage. Moreover, there was no increase in the abundance of naked cells, with a concommitant increase in the detached coccolith concentration (which indicated low coccolith detachment). For comparative purposes, we examined the same culture preserved with buffered Lugols iodine and observed detachment of coccoliths over the first 30d, such that the detached coccolith concentration *increased* 3X. Associated with this was a decrease in the number of plated coccolithophores such that, for every plated cell that became naked, there were 34 new detached coccoliths appearing in the sample. While buffered Lugols iodine does not appear to dissolve calcite coccoliths, it does appear to cause rapid detachment of coccoliths from plated cells. This problem was not apparent when using samples preserved in buffered Formalin.

Field samples showed considerably more varibility in HFALS vs. VFALS than observed for the culture-derived calcite particles. It should be noted that the HFALS gain was set 10X higher than the VFALS gain for the field samples, to make up for differences in signal strength. Field samples generally showed two distinct acid-labile populations (Fig. 10). Particles with lower HFALS were coccoliths while large HFALS particles were either large detached coccoliths or plated cells. Sorting gates were kept constant for these samples. Note, all calcite particles sorted by the flow cytometer completely dissolved upon acidification. Composition of one field sample (COBOP stn 1; Dry Tortugas; 8/20/95), was quite different from the others as it was mostly composed of aragonitic

needles in "star" clumps. These particles were presumeably resuspended from the underlying carbonate sediments.

4. Discussion

4.1 Volume Scattering Functions of Calcifying Algae

NVSF's for the various calcifying algal clones varied by a factor of ~2X overall (Fig. 2). A "generic" NVSF for calcifying algae would have great application for modeling radiative transfer within coccolithophore blooms. The average NVSF in the blue and green (normalized to the 90° value) for all the calcifying algal species, was described by the following function of Beardsley and Zaneveld [1969]:

$$\tilde{\beta}_\gamma = \beta 0 / [1 - ef \cos \gamma)^4 \, (1 + eb \cos\gamma)^4] \qquad (3)$$

where γ represented the scattering angle, while the parameters $\beta 0$, ef, and eb control the magnitude, forward lobe, and backward lobe of the NVSF, respectively. A Levenberg-Marquardt approach was used to fit this equation to the average NVSF of all the calcifying algal species. Values of $\beta 0$, ef, and eb were 1.116, -0.449, and -0.742, respectively, at 436nm, and 0.930, -0.559, and -.804, respectively, at 546nm. The average coefficient of variation for normalized $\tilde{\beta}\gamma$ measurements, for all the species, was 0.110 and 0.143 for the blue and green wavelengths respectively. Given the consistancy of the NVSF's, an average curve will be useful in predicting the optical impact of coccolithophores.

4.2 Particle-specific Backscattering

Consistancy in coccolithophore NVSF's was also apparent in the particle-specific backscattering coefficients of coccoliths from different coccolithophore clones (Fig. 3; Table 5). Differences in geometric cross-section between the coccoliths of *E. huxleyi*, *Pleurochrysis* sp., and *C. roscoffensis* were clearly not large enough to cause large variability in the particle-specific b_b* values. Note, b_b* for heavily calcified cells (with presumeably 15-30 coccoliths each) was only ~4-5X greater than for individual coccoliths, not 15-30X. We attribute this to a "self-shading effect of the attached coccoliths, such that the innermost plates were backscattering fewer photons than their external counterparts. Moreover, there was likely a competing effect of organic matter absorption, which

would lower the amount of backscattered light from particles. Also surprising, however, was that some field-derived calcite particles appeared in the same VFALS vs HFALS domain as sorted *E. huxleyi* coccoliths, but their high backscattering was more like that of plated cells. Since the particles completely disappeared upon acidification, it can be assumed that they contained no organic matter. For example, *E. huxleyi* coccoliths (Fig. 9B) and field-derived particles (Fig. 10A) had similar VFALS and HFALS characteristics, but when the scattering properties of the sorts were measured in the Wyatt light scattering photometer, the field-derived particles showed much higher backscattering cross-sections than *E. huxleyi* coccoliths (Table 5; b_b* for *E. huxleyi* clone #1516 coccoliths = 4.3 x 10^{-13} m^2 $particle^{-1}$; b_b* for Arabian Sea calcite particles from stations 1-3 = ~1.5 x 10^{-12} m^2 $particle^{-1}$). In only one field sample, were there particle-specific b_b values similar to detached coccoliths of *E. huxleyi*. Thus we can only conclude that the field-derived particles were indeed composed of calcite, with similar HFALS and VFALS (determined with the flow cytometer) but larger particle-specific backscattering than culture-derived coccoliths (determined with the Wyatt photometer). Unfortunately, to measure the calcium content of these particles required that the samples be filtered and destroyed. Hence, we do not have more definitive information on their specific identity.

4.3 Backscattering by Naked and Plated Coccolithophores

We also examined backscattering by acidified (de-plated) cells, and sorted naked cells. We have shown previously [Balch and Kilpatrick, 1996; Balch et al., 1996a and b) that acidification of seawater samples containing negligible calcite has almost no impact on the cellular backscattering. That is, for noncalcifying algae, when one subtracts the backscattering of an acidified sample from that of the total sample, the difference (b_b') is insignificantly different from zero. There have been exceptions, however, such as a region in the Equatorial Pacific along 140°W, between 6-12°S, where b_b' was a consistantly small, but negative, number [Balch and Kilpatrick, 1996]. This was inferred as resulting from populations of fragile cells that either ruptured, or deformed their shape after the pH was lowered from 8.1 to 5.6.

In experiments described here, we routinely acidified samples by CO_2 bubbling or by adding dilute glacial acetic acid, and never saw decreases in cell number, size or shape with the microscope,

save for the disappearance of the coccoliths. Interestingly, two of the calcifying algal species, *Pleurochrysis* sp. and *Thoracospaera* sp. sometimes had values of b_b' (=total b_b - acidified b_b) that were low or even negative; there was one case in which plated cells had 25% *lower* backscattering than acidified naked cells (see Fig. 6 for an example). Such a result is even more striking when compared to the 4 other calcifying clones which showed the expected 2-4X higher backscattering for plated cells than naked cells. Moreover, no decreases in cell abundance were noted for these species following acidification.

This observation illustrates the relative importance of intracellular organelles versus calcite coccoliths to overall backscattering and also illustrates a limitation to using b_b' as a proxy of calcite-dependent backscattering. Essentially, we have demonstrated that a negative b_b' for populations of *Thoracosphaera* or *Pleurochrysis* sp. does not mean cells burst, but that the calcite thecae masked a highly backscattering cellular interior. This is consistant with the optical modeling of Bricaud et al. (1992) in which the presence of internal structures markedly increased the efficiency of backscattering. Negative b_b' values in the field must be interpretted with this in mind.

4.4 Backscattering Efficiency and Particle Size

We had many opportunities to examine backscattering cross-section (b_b^*; units of m^2 $cell^{-1}$) vs. cellular geometric cross-section (same units). The slope of these plots represented the backscattering efficiency. Smallest calcite particles had largest backscattering efficiencies (Q_{bb} = 10-15% for *Cricosphaera* and 28% for *Pleurochrysis* sp. coccoliths; Fig. 11). Excepting *Thoracosphaera*, Q_{bb} values declined with increasing cross-section, approaching 1-2% for *Pleurochrysis* sp. cells. This magnitude of Q_{bb} for plated coccolithophores was predicted by Bricaud et al. (1992) using Mie theory and a 3-layered spherical model. They expected to see Q_{bb} of between 2-4% provided that the diameter of the naked cell was less than 98% of the diameter of the plated cell. Coccoliths from the *E. huxleyi* clones showed backscattering efficiencies from 5-10%; this consistancy was undoubtedly due to uniformity in shape of the *E. huxleyi* coccoliths, with any variance principally arising from experimental error. *Thoracosphaera* had higher backscattering efficiency than expected for its size. We conclude that its overall intracellular structure gave it higher backscattering efficiencies, quite apart from its calcite thecae.

Balch et al. [1996b] published scattering coefficient predictions for calcite spheres as a function of size, using anomolous diffraction theory [Van de Hulst, 1957]. Results showed peak scattering efficiency at about a 2μm diameter (see Fig. 7 of Balch et al., 1996b], with a steep decline as particles increased in size. Such results, as well as results reported here for backscattering efficiency (Fig. 11), show a similar pattern; although, it is readily admitted that there is no reason that scattering efficiency and backscattering efficiency should covary for biogenic calcite particles [Morel and Ahn, 1991], given that the VSF can show changes in the forward direction without changes in the backwards direction. For $CaCO_3$, however, this appears to be the case. Note, chlorophyll-specific scattering also increases with decreasing particle size [Morel, 1987; his Fig. 2].

4.5 Calcite-specific Backscattering Coefficient

It was clear that 30-40X variability in the particle-specific backscattering coefficient (Fig. 4) was problematic for converting oceanic b_b' values to coccolith concentration. That is, if one does not know the species of coccolithophore causing high backscattering, nor the configuration of scattering particles (detached coccoliths or plated cells), then one cannot calculate particle abundance from a backscattering measurement. Moreover, closure was difficult to achieve based on particle-specific b_b^* values (in Fig. 5, most predicted backscattering values were underestimated). This suggested that a better strategy would be to examine whether calcite-specific backscattering was uniform across the various clones of calcifying algae.

A comparison of Figs. 4 and 7 illustrates that remote sensing will be much more useful for deriving *calcite concentration* than *coccolith abundance*; while the fits within any given species were not as good in Fig. 7 as in Fig. 4, the data in Fig. 7 showed much better coherence over all species. That is, with taxonomic knowledge of the scattering species, one could explain up to 99% of the variance in calcite particle *abundance*, but without species information (generally the case with satellite remote sensing) one can explain none of the variance in particle abundance and up to 57% of the variance in *calcite concentration*. Moreover, sorts of field-derived calcite particles, followed the same trend as culture-derived particles. Finally, there was an apparent decrease in the backscattering coefficient as organic impurities increased. We can only surmise that other contaminating organic

matter absorbed some of the scattered light, thus lowering the $b_b{}^*_{Ca}$. Variation in organic matter content probably caused the 38% coefficient of variation observed on the slope in Fig. 7.

The major hurdle in the remote sensing of calcite is deriving b_b remotely. Hoge and Lyon [1996] described a method for retrieval of inherent optical properties by linear matrix inversion of satellite-derived radiance values. They estimated that total constituent backscattering at 550nm could be determined with a cumulative error of ±20%. The coefficient of determination for a calcite determination based on backscattering would then be about SQR RT(0.38^2+0.2^2) = ±43%. Obviously, it is critical that one can derive calcite-specific backscattering, distinct from the backscattering of organic matter. Gordon et al [1988] first described a scheme for deriving coccolith concentrations from estimates of blue and green reflectance (supported by fig. 8A of Balch et al., 1996b). Ackleson et al. [1994] also described a coupled atmosphere and ocean radiative transfer model to predict water-leaving radiance from a bloom of *Emiliania huxleyi*. As with the approach of Gordon et al. [1988], Ackleson et al. [1994] used an iterative approach to invert their Gulf of Maine model and simultaneously derive the chlorophyll concentration and detached coccolith concentration, ultimately based on absolute radiance measurements as opposed to radiance ratios. The fundamental issue is that given ways to resolve calcite-dependent backscattering from aircraft or satellite, then the conversion to suspended calcite concentration appears to be quite robust for a variety of species shapes, from cultured and field-derived coccoliths.

Most of the calcifying particles used in this work were either discoidal or spherical, but their size varied from ~2-18µm in diameter. When calculated on a particle-specific basis, backscattering efficiencies of calcite particles were inversely related to particle size (Fig. 11). Calcite-specific backscattering generally, but not always, increased with decreasing particle size. The one exception was for *Thoracosphera* sp. as previously noted. Variance in backscattering due to size could well explain some of the variance in the least-squares fit slope of Fig. 7.

Also clear from Fig. 7, is that the major source of variance about the least squares fit is not due to analytical error. Both the graphite furnace atomic absorption spectrometer and the light scattering photometer have coefficients of variation about ±5%. Alternatively, there may have been error due to

sample handling. Some of these samples (e.g. the flow cytometer samples) had extremely low amounts of calcite, hence some contamination cannot be ruled out. The other possibility was that variability in calcite-specific backscattering was real, due to changes in size and/or shape.

4.6 Specific Backscattering Coefficient for Organic Carbon

Interestingly, most b_b values in the literature have been normalized to chlorophyll, not organic carbon. This is because workers assumed that most scattering was due to phytoplankton and their associated debris. Morel and Ahn [1991] demonstrated the importance of other organisms to backscattering in the sea, such as bacteria and protozoa, but backscattering was not directly related to the concentration of organic carbon. Morel [1988] did show that b was approximately related to the concentration of POC. Observations of Kitchen and Zaneveld [1990] provided important links between beam attenuation or scattering versus particle volume; the latter is a short step from cellular carbon content [Strathmann, 1967]. Stramski and Reynolds [1993] implicitly made that connection when they normalized the attenuation cross section of *Thalassiosira pseudonana* to its cellular organic carbon content and were able to reduce the diurnal variability in beam attenuation by a factor of 3X. The implication is that beam attenuation and/or light scattering by phytoplankton, in general, should be highly correlated to the concentration of particulate organic carbon. Given our many b_b measurements of naked coccolithophores, we had the opportunity to examine organic carbon-specific backscattering as a function of organic carbon content of each species. Organic carbon content of cells was calculated using the plasma volume equation of Strathmann [1967; p. 411], but instead of using cylindrical volumes, spherical volumes were more appropriate for the true shape of coccolithophores and dinoflagellates. We adapted Strathmann's [1967] equation for cylinders to spheres as in equation 4.

$$Vp = \text{cell vol.} - \text{vacuole vol.} + F\,(\text{vacuole vol.}) = 4/3\,\pi\, r^3 - (1-F)\,4/3\,\pi\,(r-c)^3 \qquad (4)$$

Vp denotes plasma volume, r is the cell radius, F is the fraction of the vacuole volume that contributes to the cell carbon, and c is the thickness of the cytoplasm layer around the inside of the cell wall. The equation basically estimates plasma volume as total cell volume of a spherical cell, minus the fraction

of vacuoler volume that does not contribute any organic carbon. Using F =0.05 and c=0.16, the estimated cellular organic carbon most closely matched values for *E. huxleyi* cellular POC [Balch et al., 1992]. For the dinoflagellate, F and c were set to 0.1 and 2μm, respectively, as originally prescribed by Strathmann [1967]. Resulting particle-specific b_b^* was highly correlated to the estimated organic carbon per cell for all 5 coccolithophore species (Fig. 12). Note, the slope of this plot was equivalent to $b_b^*{}_{POC}$ and had a value of about 0.047 m^2 $(g\ C_{org})^{-1}$. The dinoflagellate *Thoracosphaera* had a higher $b_b^*{}_{POC}$ [0.115 m^2 $(g\ POC)^{-1}$].

It was possible to check the consistancy of this approach using previously published data for 22 phytoplankton species [Morel, 1987; his table 1]. We estimated plasma volume and cellular organic carbon according to Strathmann [1967] which allowed calculation of organic matter density ($c_{i\ POC}$; kg POC m^{-3} of cell volume). We multiplied Morel's b^*_{chl} values by an assumed backscattering efficiency ($\tilde{b}_b$) of 0.02, and divided this by a generic C:Chl ratio of 85, which yielded a backscattering cross-section of particulate organic matter ($b_b^*{}_{POC}$; m^2 $(g\ C)^{-1}$). The generic C:Chl value was justified in that we were able to approximate C:Chl by dividing $c_{i\ POC}$ (estimated from the Strathmann equation estimates of biomass per unit cell volume) by Morel's chlorophyll density values ($c_{i\ chl}$; kg chl m^{-3}). This yielded a median C:Chl ratio of 85 (mean = 105; std dev = 92; n = 23). Over 3/4 of the species had a $b_b^*{}_{POC}$ between 0.01 and 0.06 m^2 $(g\ C)^{-1}$, with a grand average $b_b^*{}_{POC}$ = 0.049 m^2 $(g\ C)^{-1}$ (std dev = ±0.038; n=23), quite close to our naked coccolithophore $b_b^*{}_{POC}$ of 0.047 m^2 $(g\ C)^{-1}$ (Fig. 13).

As pointed out by Morel [1987], and as observed for our naked calcifying algae, varibility in $b_b^*{}_{POC}$ was inversely correlated with particle size (Fig 14A). The inverse relationship considerably improved when the product of b_b^* and organic matter density was plotted against cell diameter (Fig 14B). De-calcified algae, save for *Pleurochrysis*, fell on the same region of the plot as other phytoplankton species. For the plated coccolithophores and detached coccoliths, plots of $b_b^*{}_{PIC}$ vs. diameter showed less size dependence (as did plots of the product, $b_b^*{}_{PIC}$ x PIC density, versus diameter; data not shown). Even though the efficiency of calcite backscattering showed some size dependence, we suggest limiting the estimate of calcite specific backscattering to an average (0.67 m^2

g PIC^{-1}), and standard deviation (0.52 m^2 g PIC^{-1}). We attribute the lesser size dependence of PIC to the fact that calcite is arranged as a "shell" around plated coccolithophores, hence calculating its effective "density" over the entire cell, and the optical consequences, is not trivial [Bricaud et al., 1992]. POC, on the other hand, is more evenly distributed throughout cells.

Knowledge of the average $b_b^*{}_{PIC}$ and $b_b^*{}_{POC}$ for marine phytoplankton is important because, if one can measure backscattering from POC and PIC, then one can derive the ratio of suspended organic carbon to inorganic carbon, long considered an important ratio for understanding vertical flux of carbon to the sea floor, not to mention its subsequent preservation [Milliman, 1993]. Clearly, particle size somewhat affects PIC backscattering (Fig. 11) but more strongly impacts POC backscattering. Knowledge of the size dependence helps interpret field backscattering measurements.

We currently can continuously measure backscattering onboard ship, before and after acidification with dilute glacial acetic acid (to dissolve suspended calcium carbonate). The prototype instrument was described previously [Kilpatrick et al., 1994; Balch and Kilpatrick, 1996]. Data shown here indicate that backscattering of acidified particles represents organic matter backscattering, while the calcite-dependent backscattering can be calculated as the difference between the b_{btotal} and $b_{bacidified}$ values. An important caveat is that acid-resistant, minerogenic particles (e.g. clay particles, opal) do not dominate the particle suite. Thus, converting $b_{bacidified}$ to POC should not be done in Case II waters [Gordon and Morel, 1982], dominated by suspended clay sediments or opal sediments, but in Case II waters over tropical carbonate banks, the technique works adequately (Balch, unpublished data). The presence of silica in diatoms might be expected to increase cellular backscattering except it is worthy of note that the diatoms examined by Morel [1987] all had lower than average backscattering per unit organic carbon, suggesting that silica frustules did not cause a large increase in their backscattering. Observations of b_{btotal} and $b_{bacidified}$ reveal the importance of $CaCO_3$ backscattering versus organic particle scattering, which is important for modeling radiative transfer [Stramski and Mobley, 1997 and Mobley and Stramski, 1997]. We are currently continuously mapping these quantities as a function of hydrography and fertility in order to better understand the PIC:POC ratio and the role of coccolithophores in the biogeochemical balance in the sea.

5. Conclusion

Acid-labile backscattering (b_b') originates mostly from calcium carbonate particles. One goal of this work was to test 2 models, one for predicting concentrations of calcite particles:

$$[\text{Coccoliths}] = b_b^*{}_{\text{partic}} \times b_b'$$

where $b_b^*{}_{\text{partic}}$ was the particle-specific backscattering coefficient. The other model was to predict the concentration of suspended calcite (particulate inorganic carbon, or PIC):

$$[\text{PIC}] = b_b^*{}_{\text{PIC}} \times b_b'$$

where $b_b^*{}_{\text{PIC}}$ was the PIC-specific backscattering coefficient. While intraspecific variance in $b_b^*{}_{\text{partic}}$ was low, interspecific variability was too great to allow accurate calculation of coccolith concentration from measurements of acid-labile backscattering. There was somewhat more intra-specific variability in $b_b^*{}_{\text{PIC}}$, but much less intra-specific variation, such that suspended calcite concentration can be calculated from acid-labile backscattering with an error of $\sim\pm 38\%$.

To test these models, plated coccolithophores and detached coccoliths were sorted with a flow cytometer, gating on the birefringence properties of $CaCO_3$. Calcite concentrations were measured with flame- and graphite-furnace atomic absorption. Results showed that coccoliths can be best sorted using HFALS and VFALS characteristics, while plated cells can be just as easily sorted using 90°LS and FALS. POC-specific backscattering coefficients ($b_b^*{}_{\text{POC}}$) of naked coccolithophores were consistent with previous results of Morel [1987] for 22 species of calcifying and non-calcifying phytoplankton, in terms of the range of $b_b^*{}_{\text{POC}}$, and their size dependence. Knowledge of $b_{b_{\text{tot}}}$, b_b', $b_b^*{}_{\text{PIC}}$, and size of organic particles appear to be sufficient to predict the PIC:POC ratio of suspended particulate matter in the sea.

Acknowledgements.

Bruce Bowler and Charlie Byrne helped with the software for processing the volume scattering data. Drs. Howard Gordon and Ken Voss provided insightful comments concerning data interpretation. Dr. Mike Sieracki helped with the flow cytometry measurments. Dr. Patricia Matrai aided in interpretation of the preservation experiments. Dr. Toby Tyrell and Dr. Andre Morel provided helpful reviews of an earlier draft of this paper. Support for this work was kindly provided by NASA (NAGW 2426; NAS5-31363), ONR (N00014-91-J-1048) and NSF (OCE-9596167) to W.M.B.. This is Bigelow Laboratory Contribution number 98002.

References

Abbott, M. R., K. H. Brink, C. R. Booth, D. Blasco, L. A. Codispoti, P. P. Niiler and S. R. Ramp, Observations of phytoplankton and nutrients from a Lagrangian drifter off northern California, *J. Geophys. Res., 95*, 9393-9409, 1990.

Ackleson, S.G., W.M. Balch, and P.M. Holligan, The response of CZCS and SeaWIFS Visible-band water-leaving radiance to particulate calcite and pigment concentration within *Emiliania huxleyi* blooms. *J. Geophys. Res. Oceans. 99*, 7483-7499, 1994.

Ackleson, S. G., and R. W. Spinrad. Size and refractive index of individual marine particulates: A flow cytometric approach. *Appl. Opt. 27*, 1270-1277, 1988.

Balch, W., M. and K. A. Kilpatrick, Calcification rates in the equatorial Pacific along 140°W. *Deep Sea Res. 43*, 971-993, 1996.

Balch, W.M., K.A. Kilpatrick, and P.M. Holligan, Coccolith formation and detachment by *Emiliania huxleyi* (Prymnesiophyceae), *J. Phycol., 29*, 566-575, 1993.

Balch, W. M., K. A. Kilpatrick, P. M. Holligan and C. Trees, The 1991 coccolithophore bloom in the central north Atlantic I- Optical properties and factors affecting their distribution, *Limnol. Oceanogr. 41*, 1669-1683, 1996a.

Balch, W. M., K. Kilpatrick, P. M. Holligan, D. Harbour, and E. Fernandez, The 1991 coccolithophore bloom in the central north Atlantic II- Relating optics to coccolith concentration. *Limnol. Oceanogr. 41*, 1684-1696, 1996b.

Balch, W. M., P. M. Holligan and K. A. Kilpatrick, Calcification , photosynthesis and growth of the bloom-forming coccolithophore, *Emiliania huxleyi., Cont. Shelf Res. 12*, 1353-1374, 1992.

Beardsley, G. F. and J. R. V. Zaneveld, Theoretical dependence of the near-asymptotic apparent optical properties on the inherent optical properties of sea water, *J. Opt. Soc. Am. 59*, 373-377, 1969.

Berger, W. H., Global Maps of Ocean Productivity, in *Productivity of the Ocean: Present and Past,* edited by W. H. Berger, V. S. Smetacek and G. Wefer, pp. 429-455, John Wiley and Sons Limited, New York, 1989.

Bricaud, A., J. R. V. Zaneveld and J. C. Kitchen. Backscattering efficiency of coccolithophorids: use of a three-layered sphere model. Ocean Optics IV, G. D. Gilbert [ed.], *Proceedings of the Society of Photo-Optical Instrumentation Engineers, 1750*, 27-33, 1992.

Brice, B. A., M. Halwer, and R. Speiser, Photoelectric light-scattering photometer for determining high molecular weights. *J. Opt. Soc. Amer. 40*, 768-778, 1950.

Broecker, W. and Peng, T. H-, *Tracers in the sea.* Lamont-Doherty Geol. Observatory, Columbia University, New York, 1982.

Brown, O. and H. Gordon, Size-refractive index distribution of clear coastal water particulates from light scattering. *Appl. Opt. 13*, 2874-2881, 1974.

Cullen, J. J., M. R. Lewis, C. O. Davis and T. R. Barber, Photosynthetic characteristics and estimated growth rates indicate grazing is the proximate control of primary production in the equatorial Pacific, *J. Geophys. Res. 97*, 639-654, 1992.

Dickey, T., J. Marra, T. Granata, C. Langdon, M. Hamilton, J. Wiggert, D. Siegel and A. Bratkovich, Concurrent high resolution bio-optical and physical time series observations in the Sargasso Sea during the spring of 1987, *J. Geophys. Res. 96*, 8643-8664, 1991.

Fernandez, E., P. Boyd, P. M. Holligan and D. S. Harbour. Production of organic and inorganic carbon within a large scale coccolithophore bloom in the north Atlantic Ocean. *Mar. Ecol. Prog. Ser., 97*, 271-285, 1993.

Fleming, R. H., General features of the ocean, in *Treatise on Marine Ecology and Paleoecology*, edited by J. W. Hedgpeth, *Geological Society of America Memoir 67*, 87-107, 1957.

Gardner, W. D., S. P. Chung, M. J. Richardson, and I. D. Walsh, The oceanic mixed-layer pump, *Deep-Sea Res. 42*, 757-775, 1995.

Gardner, W. D., I. D. Walsh, and M. J. Richardson, Biophysical forcing of particle production and distribution during a spring bloom in the North Atlantic. *Deep-Sea Res. II, 40*, 171-195, 1993.

Gordon, H., Radiative transfer in the ocean: A method for determination of absorption and scattering properties, *Appl. Opt. 15*, 2611-2613, 1976.

Gordon, H. R., O. B. Brown, R. H. Evans, J. W. Brown, R. C. Smith, K. S. Baker, and D. K. Clark, A semianalytic radiance model of ocean color, *J. Geophys Res. 93*, 10,909-10,924, 1988.

Gordon, H. R. and A. Y. Morel, Remote assessment of ocean color for interpretation of satellite visible imagery- a review. in *Lecture Notes on Coastal and Estuarine Studies*, edited by R. T. Barber, C. N. K. Mooers, M. J. Bowman, and B. Zeitzschel, 114 pp., Springer-Verlag, New York, 1983.

Hoge, F. E., and P. E. Lyon, Satellite retrieval of inherent optical properties by linear matrix inversion of oceanic radiance models: An analysis of model and radiance measurement errors, *J. Geophys. Res. 101*, 16,631-16,648, 1996.

Keller, M. D., R. C. Selvin, W. Claus, and R. R. L. Guillard, Media for the culture of oceanic ultraphytoplankton, *J. Phycol. 23*, 633-638, 1987.

Kiefer, D. A. and R. W. Austin, The effect of varying phytoplankton concentration on submarine light transmission in the Gulf of California. *Limnol. Oceanogr. 19*, 55-64, 1974.

Kilpatrick, K. A., Y. Ge, W. M. Balch, and K. Voss, The "Ge Meter": A photometer for the continuous measurement of calcite-dependent light scatter in seawater, *Society of Photo-Optical Instrumentation Engineers, 2258*, 512-521, 1994.

Kirk, J. T. O., *Light & Photosynthesis in Aquatic Ecosystems*, 2nd ed., Cambridge University Press, New York, 1994.

Kitchen, J. and R. Zaneveld, On the noncorrelation of the vertical structure of light scattering and chlorophyll a in case I waters, *J. Geophys. Res. 95*, 20,237-20,246, 1990.

Koblentz-Mishke, O. I., V. V. Volkovinsky, and J. G. Kabanova, Plankton primary production of the world ocean, in *Scientific Exploration of the South Pacific* , edited by W. Wooster, pp. 183-193, National Academy of Sciences, Washington, D. C., 1970.

Lieth, H. and R. H. Whittaker, *Primary Productivity of the Biosphere*, Springer-Verlag, New York, 1975.

Longhurst, A., S. Sathyendranath, T. Platt, and C. Caverhill, An estimate of global primary production in the ocean from satellite radiometer data. *J. Plank. Res. 17*, 1245-1271, 1995.

Milliman , J. D., Production and accumulation of calcium carbonate in the ocean: budget of a nonsteady state. *Global Biogeochem. Cycles. 7*, 927-957, 1993.

Mobley, C. D. and D. Stramski, Effects of microbial particles on oceanic optics: Methodology for radiative transfer modeling and example simulations, *Limnol. Oceanogr., 42*, 550-560, 1997.

Morel, A., 1987. Chlorophyll-specific scattering coefficient of phytoplankton, a simplified theoretical approach. *Deep Sea Res. 34*, 1093-1105.

Morel, A. 1988. Optical modeling of the upper ocean in relation to its biogenous matter content (case 1 waters). J. Geophys. Res. 93: 10749-10768.

Morel, A. and Y. Ahn, Optics of heterotrophic nanoflagellates and ciliates: A tentative assessment of their scattering role in oceanic waters compared to those of bacterial and algal cells. *J. Mar. Res., 49*, 177-202, 1991.

Moshkovitz, Shimon and K. Osmond, The optical properties and microcrystallography of Arkhangelskiellaceae and some other calcareous nannofossils in the Late Cretaceous, in *Nannofossils and their applications*, edited by J. A. Crux and S. E. van Heck, pp. 76-97, Ellis Horwood, Chichester, 1989.

Olson R., E.R. Zettler, and O.K. Anderson, Discrimination of eukaryotic phytoplankton cell types from light scatter and autofluorescence properties measured by flow cytometry, *Cytometry 10*, 636-643, 1989.

Paasche, E., Coccolith formation, *Nature 193*, 1,094-1,095, 1962.

Pak, H., The Columbia River as a source of marine light scattering particles, Ph.D. Thesis, Oregon State University, Corvalis, 1970.

Pak, H., D. A. Kiefer and J. C. Kitchen, Meridional variations in the concentration of chlorophyll and microparticles in the North Pacific Ocean, *Deep-Sea Res. 35*, 1,151-1,171, 1988.Platt, T. and D. V. Subba Rao, Primary production of marine microphytes. Photosynthesis and productivity in different environments, in *International Biological Programme*, Cambridge Univ. Press, Cambridge, England, *3*, pp. 249-279, 1975.

Press, W. H., B. P. Flannery, S. A. Teukolsky, and W. T. Vetterling, *Numerical Recipes*, Cambridge University Press, N.Y., 1989.

Richardson, M. J., W. D. Gardner, S. P. Chung and I. D. Walsh, Source of beam attenuation signal as a function of particle size (abstract), The Oceanogr. Soc. Meeting, Seattle, WA, pp. 71, 1993.

Ryther, J. H., Photosynthesis and fish production in the sea, *Science 166*, 72-76, 1969.

Seibold, E. and W. H. Berger, *The sea floor- An introduction to marine geology*. Springer-Verlag, New York, 1982.

Siegel, D. A., T. D. Dickey, L. Washburn, M. K. Hamilton, and B. G. Mitchell, Optical determination of particulate abundance and production variations in the oligotrophic ocean, *Deep-Sea Res. 36*, 211-222, 1989.

Spilhaus, A. F. Jr., Observations of light scattering in sea water. Ph.D. thesis, Massachusetts Institute of Technology, Cambridge, 1965.

Spinrad, R. and J. R. V. Zaneveld, An analysis of the optical features of the near-bottom and bottom nepheloid layers in the area of the Scotian rise, *J. Geophys Res. 87*, 9,553-9,561, 1982.

Steemann Nielsen, E., On organic production in the oceans. *Conseil Perm. Intern. Explor. Mer., J. du Conseil, 19*, 309-328, 1954.

Stramski, D. and C. D. Mobley, Effects of microbial particles on oceanic optics: A database of single-particle optical properties, *Limnol. Oceanogr., 42*, 538-549, 1997.

Stramski, D. and R. A. Reynolds, Diel variations in the optical properties of a marine diatom, *Limnol. Oceanogr. 38*, 1,347-1,364, 1993.

Strathman, R. R., Estimating the organic carbon content of phytoplankton from cell volume or plasma volume. *Limnol. Oceanogr. 12*, 411-418, 1967.

Tangen, K., L. E. Brand, P. L. Blackwelder and R. R. L. Guillard, Thoracosphaera heimii (Lohmann) Kamptner is a dinophyte: Observations on its morphology and life cycle. *Mar. Micropal.* *7*, 193-212, 1982.

Van de Hulst, H. C. *Light scattering by small particles*, John Wiley, New York, 1957.

Walsh, I. D. Project CATSTIX: Camera, transmissometer and sediment trap integration experiment, Ph.D. thesis, Texas A&M University, College Station, TX, 1990.

Westbroek, P., C. W. Brown, J. van Blejswijk, C. Brownlee, G. Brummer, M. Conte, J. Egge, E. Fernandez, R. Jordan, M Knappertsbusch, J. Stefels, M. Veldhuis, P. van der Wal, and J. Young, A model system approach to biological climate forcing. The example of *Emiliania huxleyi*, *Global and Planetary Change.* *8*, 27-46, 1993.

Zaneveld, J. R. V., D. M. Roach, and H. Pak, The determination of the index of refraction distribution of oceanic particulates, *J. Geophys. Res.* *79*, 4091-4095, 1974.

Table 1- Calcifying algal clones used in experiments. The CCMP culture number is given when available.

Species	Bigelow Lab Culture Collection Number	Collection Site	Growth Temperature
Emiliania huxleyi ("88E")	CCMP 378	Gulf of Maine	15-16
Emiliania huxleyi ("88E-1/2-5")	NA†	Gulf of Maine	15-16
Emiliania huxleyi ("89E")	CCMP 374	Gulf of Maine	15-16
Emiliania huxleyi	CCMP 1516	2°40'S x 82°43'W	15-16
Thoracosphaera sp.§	CCMP 1070	32° 53' x 68°W	21
Syracosphaera elongata ("SE62")	CCMP 874	NA	15-16
Pleurochrysis sp.§	CCMP 299	NA	21
Coccolithus neohelis	CCMP 298	La Jolla, CA	15-16
Cricosphaera roscoffensis§	CCMP 1588	Narragansett Bay, RI	21

† Balch collection
§Grown on shaker table.

Table 2- Experimental details used for sorting particles with EPICS V flow cytometer, measuring the particulate calcium concentration, and calcite volume scattering. Scattering due to coccoliths estimated by 1) making sequential additions of coccoliths to light scattering photometer cuvette, or 2) measuring scattering before and after dissolution of calcium carbonate coccoliths. Method of dissolution given in column 3. In all experiments, particle enumeration was performed with an Olympus BH2 microscope equipped with polarization optics and epifluorescence. Moreover, such cell counts served as a control to verify that, following acidification, cell concentration was unaffected and all calcite dissolved. See text for more details.

Exp.		*Particle Sorting & Handling*			*Light Scattering Measurements*			
Design/ Particles Sorted	Species	Coccolith dissolution	sorting criteria	Partic. Ca analysis	Inst.	vol. cuvette (ml)	wavelen. (nm)	closure examined
1 Pltd Cells	*E. huxleyi* (88E) *S. elongata* *Pleurochrysis* sp. *Thoracosphaera.* sp.	30s CO_2 bubbling§	FALS* 90° vol scat** LIRFI***	none	Brice Phoenix∞	30ml	436 546	yes
2 Liths	*E. huxleyi* clone 88E *E. huxleyi* clone 89E *Thoracosphaera* sp. *Pleurochrysis* sp. *C. neohelis* *S. elongata* *C. roscofensis*	GAA‡	FALS* 90° vol scat**	AA§§	Wyatt†	10ml	632.8	yes
3 Liths	*E. huxleyi* clone 88E *E. huxleyi* clone 89E *E. huxleyi clone 1516* *Cricosphaera roscoffensis* *Thoracosphaera* sp.	GAA‡	HFALS~ VFALS~	GFAA¤	Wyatt†	10ml	632.8	no
4 Liths	Natural samples preserved in buffered Formalin	GAA‡	HFALS~ VFALS~	GFAA¤	Wyatt†	10ml	632.8	no

*Forward angle light scattering (range=1.5°-19°)

**90° volume scattering (range=73°-107°, also referred to as "side scattering")

*** Laser Induced Red Fluorescence

**Brice Phoenix model 2000 light scattering photometer [Brice et al., 1950]. Volume scattering measurements made as described in Balch et al., [1996a]. See also Spilhaus [1965], and Pak [1970] for discussions on accuracy and precision. 30mL samples placed in a 6-sided glass cuvette designed for sampling at 45°, 90° and 135°. Instrument calibration performed with an opal glass reference and working standard. Calibration constants checked routinely to determine instrument stability. Checks on calibration and absolute accuracy checked with 0.2µm-filtered Milli-Q water several times daily. Dark current measurements performed after every sample. Volume scattering of blank seawater measured before addition of any particles. This allowed verification of instrument calibration, as well as subsequent subtraction of water scattering for calculation of particle-specific scattering coefficients. Containment effects were negligible, in agreement with Spilhaus [1965], who demonstrated containment negligible effects provided storage time was ≤ 1h (he took readings at 5° intervals, from 30°-135° thus his sampling time was potentially longer than ours). Cylindrical cuvette used to measure VSF in 5° increments between 30° and 135°. Total backscattering calculated by fitting Beardsley-Zaneveld [1969] function to volume scattering data at 45°, 90°, and 135°. Fitted Beardsley-Zaneveld function then integrated, between 90°-180° to estimate total backwards scattering.

§To verify that microbubbles were not increasing volume scattering, controls run in which filterred seawater was bubbled with CO_2 prior to scattering measurements. No significant differences were noted. Volume scattering measurements were repeated on the de-calcified samples.

‡ 1% glacial acetic acid added to seawater/particle suspension to final concentration of 1.33×10^{-2}% by volume.

§§ Analysis according to Fernandez et al. [1993] and Kilpatrick et al. [1994]. Calcite particles filtered onto baked GFF filters. Ca measured using a Perkin Elmer model 2380 flame-atomic absorption spectrometer with 10 cm flame, and 422.7nm incident beam. Calibrated with Fisher Ca standard.

†Wyatt Technologies Dawn Laser Light-Scattering Photometer used for measurement of VSF at 15 angles (35.5°, 39.8°, 45.0°, 51.3°, 59.0°, 68.2°, 78.7°, 90.0°, 101.3°, 111.8°, 121.0°, 128.7°, 135.0°, 140.2°, and 144.5°) at 400 Hz, averaged over 20s. Light source was a He-Ne laser (632.8 nm). Instrument calibrated at 90° using a solid scattering standard. Detector signals "normalized" with isotropic glass scattering standard. Total backscattering calculated by integrating volume scattering from 90°-144.5° using standard trapezoidal integration. Integration of scattering from 144.5° to 180° accomplished by fitting Beardsley-Zaneveld [1969] function to volume scattering data at 45°, 90°, and 135°. Beardsley-Zaneveld function then integrated, and two integrals (90°-144.5° and 144.5°-180°) summed to estimate total backwards scattering. Difference between integrating using above method, versus simply integrating the fitted Beardsley-Zaneveld function between 90°-180°, showed differences <5%, in accordance with observations of Gordon (1976; his Table 1). Volume scattering measurements of culture samples performed with 3-5 replicates. Samples swirled routinely or stirred with a microstirrer to maintain particles in suspension. Gaussian beam diameter of laser = 0.39mm. Scattering volume illuminated by laser (and viewed by photodetectors) =0.031µl.

~ VFALS=vertically-polarized forward angle light scattering; HFALS= horizontally-polarized forward angle light scattering.

¤ After last serial addition of coccoliths, and VSF measurement, sample was filtered onto a 13 mm 0.2µm pore-size polycarbonate filter, rinsed with borate buffer to remove all traces of dissolved Ca, and frozen in acid-cleaned centrifuge tubes for later analysis. Ca concentrations determined with a Perkin Elmer model Z5100 graphite furnace atomic absorption spectrometer. Sample dissolved in 5 ml 0.5% Optima grade nitric acid in distilled water. Instrument auto sampler then diluted with same acid to a final Ca concentration <0.37 µM before injection into the graphite furnace. Analytical sensitivity= 2.5 nM.

Table 3- Notation

β_γ	Volume scattering at angle γ, m^{-1} sr^{-1}
$\beta 0$	Parameter for fitting magnitude of volume scattering function
$b_{b\ total}$	Total backscattering coefficient of untreated seawater, m^{-1}
$b_{b\ acidified}$	Backscattering coefficient of acidified solution (pH~5.6)
b_b'	Difference between bb_{total} and $bb_{acidified}$; acid labile backscattering, m^{-1}
$b_{b\ pred}$	Backscattering predicted from the sum of the backscattering by j particle types, m^{-1}
$b_b{}^*_{partic}$	Particle backscattering crossection, m^2 (particle)$^{-1}$
$b_b{}^*cc$	Particle backscattering crossection, m^2 (particle)$^{-1}$, where particle concentration was calculated from microscope counts
$b_b{}^*FCM$	Particle backscattering crossection, m^2 (particle)$^{-1}$, where particle concentration was calculated from the flow cytometer
$b_b{}^*Ca$	Calcite backscattering crossection, m^2 (mg calcite C)$^{-1}$ or m^2 (mol Ca)$^{-1}$
$b_b{}^*_{POC}$	Particulate organic C backscattering crossection, m^2 (mg POC)$^{-1}$
$\tilde{b_b}$	Ratio of backscattering to scattering, ("backscattering probability")
c	Thickness of cytoplasm layer (m)
$c_{i\ POC}$	Density of organic matter (kg m^{-3})
c_j	Concentration of jth particle type, number m^{-3}
C_{CaCO_3}	Concentration of calcium carbonate, mg calcite C m^{-3}
e_b	Parameter for fitting backwards lobe of volume scattering function
e_f	Parameter for fitting forwards lobe of volume scattering function
F	Fraction of the vacuolar volume contributing cellular organic carbon
HFALS	Horizontally-polarized forward angle light scattering, relative units
POC	Particulate organic carbon, g organic carbon m^{-3}
Q_{b_b}	Backscattering efficiency
r	Cell radius, m

VFALS	Vertically-polarized forward angle light scattering, relative units
Vp	Plasma volume (m^3)

Table 4- Location and depths of field samples pooled and subsampled for determination of calcite-specific backscattering coefficients. "UW" denotes underway sample from ship's seawater system as opposed to a Niskin sample on station.

Sample	Stn	Location	N. Lat	Lon	Date DMY	Time UDC	Depth (m)
1	3	Arabian Sea	21.8°	62.4°E	19Jul95	0136	1,5,11,18,27,37,45,65
2	1	Arabian Sea	22.4°	59.9°E	18Jul95	0426	1,2,4,6,9,13,16,23
	3	Arabian Sea	21.8°	62.4°E	19Jul95	0136	1,5,11,18,27,37,45,65
3	10	Arabian Sea	16.3°	68.4°E	24Jul95	1558	1,4,12,19,27,38,46,66
4	14	Arabian Sea	13.2°	65.0°E	28Jul95	2357	1,4,12,19,27,38,46,66
	15	Arabian Sea	12.0°	65.0°E	29Jul95	1223	1,5,14,23,33,47,56,81
	16	Arabian Sea	10.8°	65.0°E	30Jul95	0031	1,5,14,23,33,47,56,81
	17	Arabian Sea	10.0°	64.9°E	30Jul95	2208	1,4,12,20,28,40,48,69
5	18	Arabian Sea	14.4°	65.0°E	2Aug95	0724	1,4,12,20,28,40,48,69
	21	Arabian Sea	15.6°	62.8°E	3Aug95	1215	1,4,12,20,28,40,48,69
	30	Arabian Sea	18.5°	57.3°E	11Aug95	2231	1,3,7,11,16,22,27,38
	32	Arabian Sea	18.8°	58.2°E	12Aug95	1939	3,13,23,33,43,52,62
	uw	Arabian Sea	15.0°	66.4°E	26Jul95	0238	1
	uw	Arabian Sea	15.1°	66.1°E	26Jul95	0431	1
	uw	Arabian Sea	15.3°	65.7°E	26Jul95	0646	1
	uw	Arabian Sea	15.4°	65.2°E	26Jul95	0930	1
	uw	Arabian Sea	15.2°	64.9°E	26Jul95	1130	1
	uw	Arabian Sea	15.6°	64.5°E	26Jul95	1330	1
	uw	Arabian Sea	15.8°	64.2°E	26Jul95	1625	1
	27	Arabian Sea	17.2°	59.9°E	7Aug95	0925	48
	uw	Arabian Sea	17.2°	59.8°E	8Aug95	1722	1
	uw	Arabian Sea	17.4°	59.4°E	8Aug95	1925	1

	uw	Arabian Sea	17.4°		59.5°E	8Aug95	2135	1
6	1	Dry Tortugas	24.6°		82.9°W	20Aug95	1445	1

Table 5- Particle- and calcite-specific backscattering coefficients calculated from all experiments. A "total" sample indicates the b_b of a mixture of cells and detached coccoliths (POC & PIC). "Acid labile" indicates the backscattering from just calcite (the difference in backscattering between the total particle suspension and the de-calcified, acidified suspension). Thus, a $b_b{}^*_{Ca}$ for the "total" sample was calculated as the b_b from calcite and organic matter in the total sample, normalized to the concentration of particulate calcium (calcite). The $b_b{}^*_{Ca}$ for "acid-labile" particles was calculated as the the difference between total and acidified b_b, normalized to the concentration of suspended calcium in the original sample. Sample filtrations ("lith filtrates") were made using 1µm filters. "AS" denotes Arabian Sea samples.

		$b_b{}^*_{particle}$ (m^2/particle)			$b_b{}^*_{Ca}$ (m^2/mol Ca)		
		436 nm	546 nm	632 nm	436 nm	546 nm	632 nm
Emiliania huxleyi 88E	Heavy plated cells	3.74E-12	3.10E-12	1.06E-12			
	Naked cells‖	9.90E-13	9.50E-13	3.60E-13			
	Coccoliths‖	1.40E-13	1.30E-13	2.24E-13			
	Total	4.65E-12	4.52E-12				4.22
	Acid labile						2.82
Emiliania huxleyi 89E	Plated cells			1.07E-12			
	Naked cells			2.96E-13			
	Coccoliths			2.72E-13			
	Total 36ml lith filtrate			3.97E-13			7.10
	Total 50ml lith filtrate			5.15E-13			15.5
	Total 144ml lith filtrate			2.32E-13			14.9
	Pure lith sort&PCa			3.08E-13			28.4
	Total						2.27
	Acid labile						1.35
Emiliania huxleyi CCMP 1516	Coccoliths			3.85E-13			
	Coccoliths			4.79E-13			
	Coccoliths			4.41E-13			8.54
BOFS *Emiliania huxleyi* bloom †	acid-labile	1.84E-13	1.35E-13		2.11	1.63	
Pleurochrysis sp.	Plated cells	3.43E-12	3.23E-12	4.13E-12			
	Naked cells	3.00E-12	2.52E-12	2.60E-12			
	Coccoliths	9.81E-13	8.74E-13	5.71E-13			
	Total	6.23E-12	6.09E-12				7.14
	Acid-labile						4.50
Cricosphaera roscoffensis	Plated cells			5.21E-12			
	Coccoliths			3.79E-13			8.08
	Total 15ml lith filtrate			3.92E-13			9.91
	Total 25ml lith filtrate			4.31E-13			11.2
	Total 35ml lith filtrate			2.63E-13			12.5
	Total						5.61
Syracosphaera sp.	Plated cells	5.23E-12	3.42E-12				
	Naked cells	3.17E-12	2.73E-12				
	Coccoliths	7.56E-13	2.21E-12				
	Total	4.23E-12	3.83E-12				4.84
	Acid-labile						2.41
Thoracosphaera sp.	Thecate cells	4.45E-12	1.78E-12	1.10E-11			17.2
	Naked cells	4.23E-11	2.90E-11	7.67E-12			
	Empty thecae	5.92E-12	2.40E-12	8.77E-12			12.4
	Sm. thecate cells			6.18E-12			
	Lg. thecate cells			7.35E-12			
	Total 60ml	1.07E-11	8.84E-12	4.95E-12			5.84
	Total						12.6
AS Stn10	Sm. CaCO3 particles			9.43E-13			10.6
	Lg. CaCO3 particles			7.07E-13			10.4
AS Stns14,15,16,17	Sm. CaCO3 particles			2.07E-13			3.02
	Lg CaCO3 particles			9.12E-13			3.63
AS Stns 1&3 rep1 ~	Sm. CaCO3 particles			1.35E-12			
	Lg. CaCO3 particles			4.27E-12			
AS Stns 1&3 rep2	Sm. CaCO3 particles			1.85E-12			8.84
	Lg. CaCO3 particles			6.70E-12			3.88
Dry Tortugas STN 1(8/20/95)				7.90E-12			6.73
AS stn 18,21,30,32,+2 UW's(3-10um)	Sm. CaCO3 particles			1.00E-12			9.65
	Lg. CaCO3 particles			5.03E-12			8.55
Average		5.88E-12	4.46E-12	2.55E-12	2.11	1.63	8.53
Std Dev		9.75E-12	6.68E-12	3.04E-12			5.58

† Data taken from Balch et al. (1996b)
‖ Values at 436nm and 546nm from Voss et al. (in press)

Figure Legend

Fig. 1- Scanning electron micrographs of calcifying algae used in these experiments. The diameter of each cell and coccolith respectively is: A) *E. huxleyi* clone 88E=6.4μm & 2.5μm (scale bar = 1μm); B)*C. roscoffensis*=13.6μm & 1.77μm (scale bar = 10μm); C)*Pleurochrysis* sp.=18μm & 1.6μm (scale bar = 10μm); D)*C. neohelis*=18μm & 2.1μm (scale bar = 5μm); E)*Thoracosphaera* sp thecae= 11μm (scale bar = 10μm); Not shown- *E. huxleyi* clone 89E = 5.5μm cell & 2.5μm coccolith. *Syracosphaera* sp. = 18μm cell & 2.1μm coccolith.

Fig. 2- Normalized volume scattering functions of four calcifying algal strains (normalized to $\beta 90^{o}$. Symbols denote: ▲=*E. huxleyi*, ▼ = *S. elongata*; ■ =*Pleurochrysis* sp.; ● = *Thoracosphaera* sp. Open and closed symbols represent 436nm and 546nm volume scattering respectively. These data were collected using experimental design number 1 (see methods).

Fig. 3- Histogram of particle-specific b_b^* (632.8 nm) for different species of calcifying algae as well as field-derived calcite particles. Same data as shown in Table 5. These data were collected using experimental design numbers 2-4 (see Table 2).

Fig. 4- Plots of backscattering at 632.8 nm versus particle concentration for *E. huxleyi* coccoliths (clone 89E), *Cricosphaera* sp. coccoliths, and *Thoracosphaera* thecae. The slopes for the three species were was as follows: O=*Thoracosphaera* sp.= 1.08×10^{-11} m^2 $coccolith^{-1}$, r^2=0.869; Δ= *Cricosphaera* = 4.27×10^{-13} m^2 $coccolith^{-1}$, r^2=0.999; and ●=*E. huxleyi* = 3.56×10^{-13} m^2 $coccolith^{-1}$, r^2=0.994. Error bars represent one standard deviation about the mean. These data were collected using experimental design number 3 (see methods).

Fig. 5- Measured vs predicted bb for 7 different calcifying algal clones. Species denoted as follows: *E. huxleyi* clone 88E= ★; *E. huxleyi* clone 89E=●; *Thoracosphaera* sp.= ■; *Pleurochrysis* sp.=✚; *C. neohelis*= ▲; *S. elongata* = ◆; and *C. roscofensis* = ▼. Closed and open symbols indicate calcified and decalcified cells respectively. These data were collected using experimental design number 2 (see methods).

Fig. 6- Histogram of Qbb plated/Qbb naked for 6 species of calcifying algae. The Qbb plated/Qbb naked value of 1 is shown for reference. These data were collected using experimental design number 2 (see methods).

Fig. 7- Backscattering vs calcite concentration (mol m^{-3}) for bulk culture samples (open symbols) and flow cytometer sorts (solid symbols). These data were collected using experimental design numbers 2-4 (see methods). Measurements of field particles are denoted with black numbered circles. At seawater coccolith concentrations, field samples had to be filter concentrated before running through the flow cytometer. In most cases, samples from several stations were combined to have sufficient numbers of particles for sorting. Error bars represent one standard deviation. When error bars are not shown, they are smaller than the symbol on the plot. Species denoted as follows: *E. huxleyi* clone 88E= ★; *E. huxleyi* clone 89E=●; *Thoracosphaera* sp.= ■; *Pleurochrysis* sp.=✚; *S. elongata* = ◆; and *C. roscoffensis* = ▼. Field sample results denoted as follows: ❶=Arabian Sea Stn 10 small; ❷ = Arabian Sea Stn 10 large; ❸= Arabian Sea Stn 14-17 small; ❹= Arabian Sea Stn 1 and 3 small; ❺ = Arabian Sea Stn 1 and 3 large, ❻= CoBop Stn 1, ❼ = Arabian Sea Stns 18, 21, 30, 32 small; ❽ = Arabian Sea Stns 18, 21, 30, 32 large.

Fig. 8- Flow cytometer scatter plots for calcifying algal strains A) *Syracosphaera*, B) *Pleurochrysis* sp., C) *Thoracosphaera*, and D) *E. huxleyi* clone 88E. Solid lines represent population distributions of untreated plated cells. Dashed lines represent distributions of cells following bubbling with CO_2 to drop the pH and dissolve coccoliths. Flow cytometer analysis for the acidified *E. huxleyi* cells was lost (hence, no dashed lines are shown in panel 8D). The hatched regions represent the sorting gates used for plated cells only. Two sorting gates are shown in panels C and D, in which there were clearly two populations evident. These data were collected using experimental design number 1 and 2 (see methods).

Fig. 9- Flow cytometer scatter plots for A) *E. huxleyi* , clone 89E detached coccoliths, B) *E. huxleyi* , CCMP clone 1516 detached coccoliths and plated/naked cells, C) *Cricosphaera roscofensis* detached coccoliths, and D) empty *Thoracosphaera* sp. thecae. The plots show the particle distributions for VFALS versus HFALS. The hatched regions represent the sorting windows for these particles. Dashed lines represent the remaining population distributions following acidification. No particles were observed after acidification of *C. roscoffensis* coccoliths (panel C). These data were collected using experimental design number 3 (see Table 2). Numbers along both axes represent relative values only within each channel. No interchannel comparisons can be made. Since HFALS was considerably lower than VFALS, the gain for the HFALS detector was set 5X greater than for VFALS except for *E. huxleyi* clone #1516, where the HFALS gain was set 10X higher than the VFALS gain.

10) Flow cytometer scatter plots for field-derived calcite particles. Panels show the particle distributions for VFALS versus HFALS for 4 aggregate samples from the Arabian Sea (JGOFS Process cruise 4; see table 4 for locations): A) stations 1-3, all depths B) station 10, all depths, C) stations 14-17, all depths, and D) stations 18, 21, 30, 32, and 2 surface underway samples(3-10μm size fraction only). Hatched patterns represent sorting gates. These data were collected using experimental design number 4 (see methods). Absence of dashed lines (panel A) means all particles disappeared upon acidification.

Fig. 11- Plot of backscattering efficiency (Qbb) versus particle diameter. Open symbols=coccoliths or empty calcite thecae, closed symbols=plated cells; Species--▼=*E. huxleyi* clone 88E, ▲=clone 89E, ■=clone CCMP1516; ●=*Pleurochrysis* sp., ◆=*C. roscoffensis*; ✦=*Thoracosphaera* sp. These data were collected using experimental design number 1-3 (see methods).

Fig. 12- - Backscattering cross section versus estimated cellular organic carbon content for several species of "naked" calcifying algae (i.e. calcite removed by acid addition). Symbols: ★=*E. huxleyi* clone 88E, O=clone 89E; ✦=*C. pelagicus*, ▼=*C. roscofensis*; ■=*Thoracosphaera* sp., ◆=*S.*

elongata. Line drawn only for coccolithophore species. These data were collected using experimental design number 2 (see methods).

Fig. 13- Histogram showing predicted $b_b^*{}_{POC}$ values for 22 species listed in Morel [1987; his table 1). Calculations assume a C/Chl ratio of 85, and a value of $\tilde{b}_b$ of 0.02. Cumulative frequency distribution also shown.

Fig. 14- Re-interpretation of table 1 from Morel [1987] in which chlorophyll-specific scattering cross-section for 22 species of phytoplankton (filled squares) was converted to a POC-specific backscattering cross-section, assuming a C:Chl ratio of 85 and backscattering efficiency ($\tilde{b}_b$) of 2%. Values of $b_b^*{}_{632}$ for the calcifying algal species used in our experiments designated with open triangles. The high outlier at 18μm diameter is from *Pleurochrysis*. b) Cellular backscattering coefficient (product of POC density (g POC m^{-3}) and the POC-specific backscattering cross-section (m^2 (g POC)$^{-1}$) plotted as a function of particle size for the same species given in panel a (same symbols). This format condensed data of panel a into a tighter curve, save for *Pleurochrysis*, also discussed by Morel [1987].

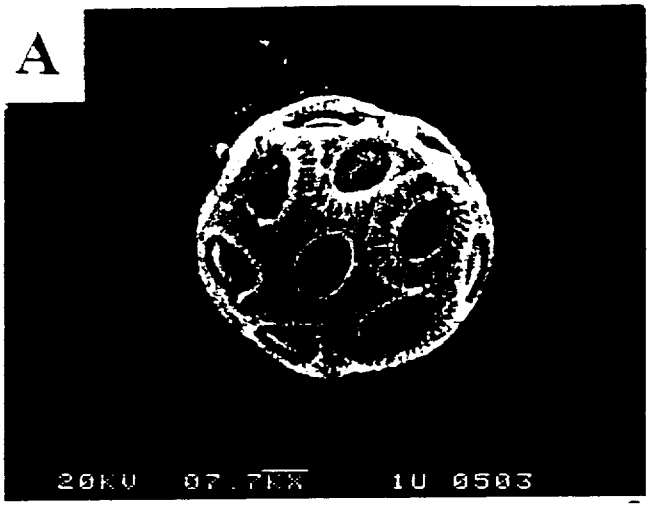
A
20KV 07.7KX 1U 0503

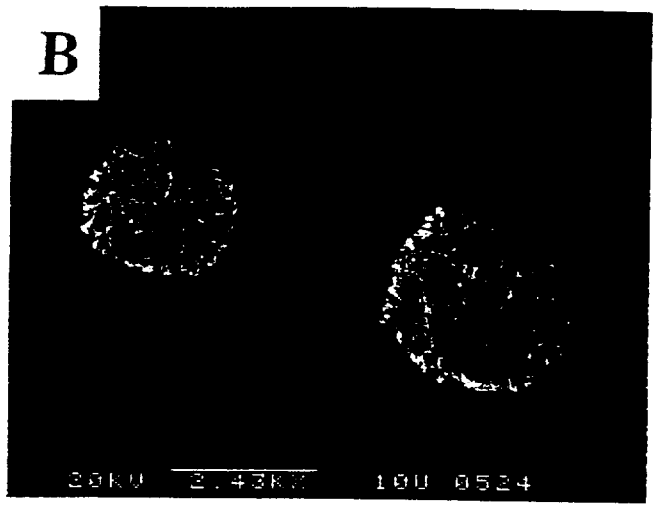
B
20KV 2.43KX 10U 0524

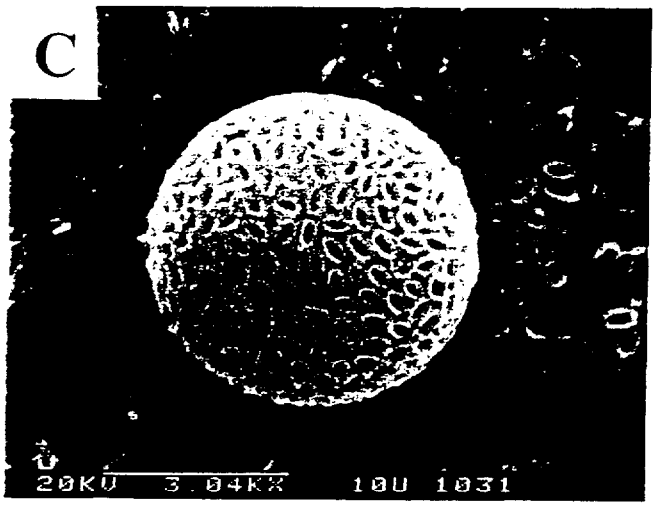
C
20KV 3.04KX 10U 1031

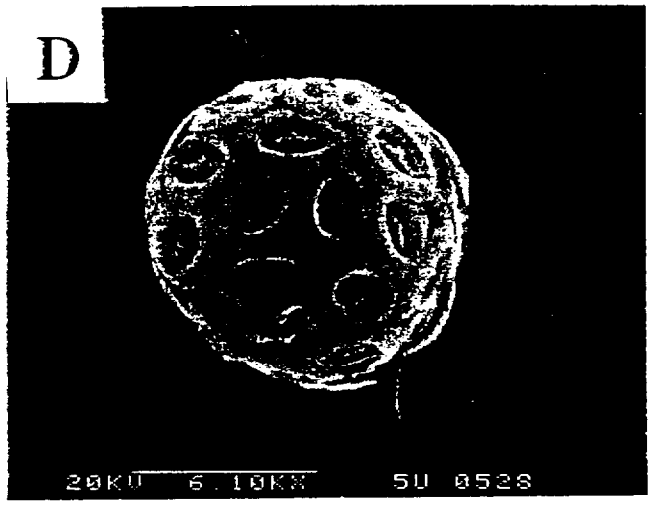
D
20KV 6.10KX 5U 0528

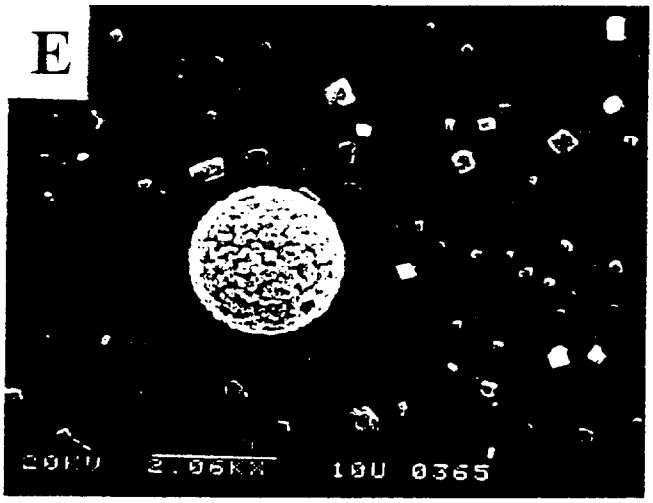
E
20KV 2.06KX 10U 0365

Fig. 1

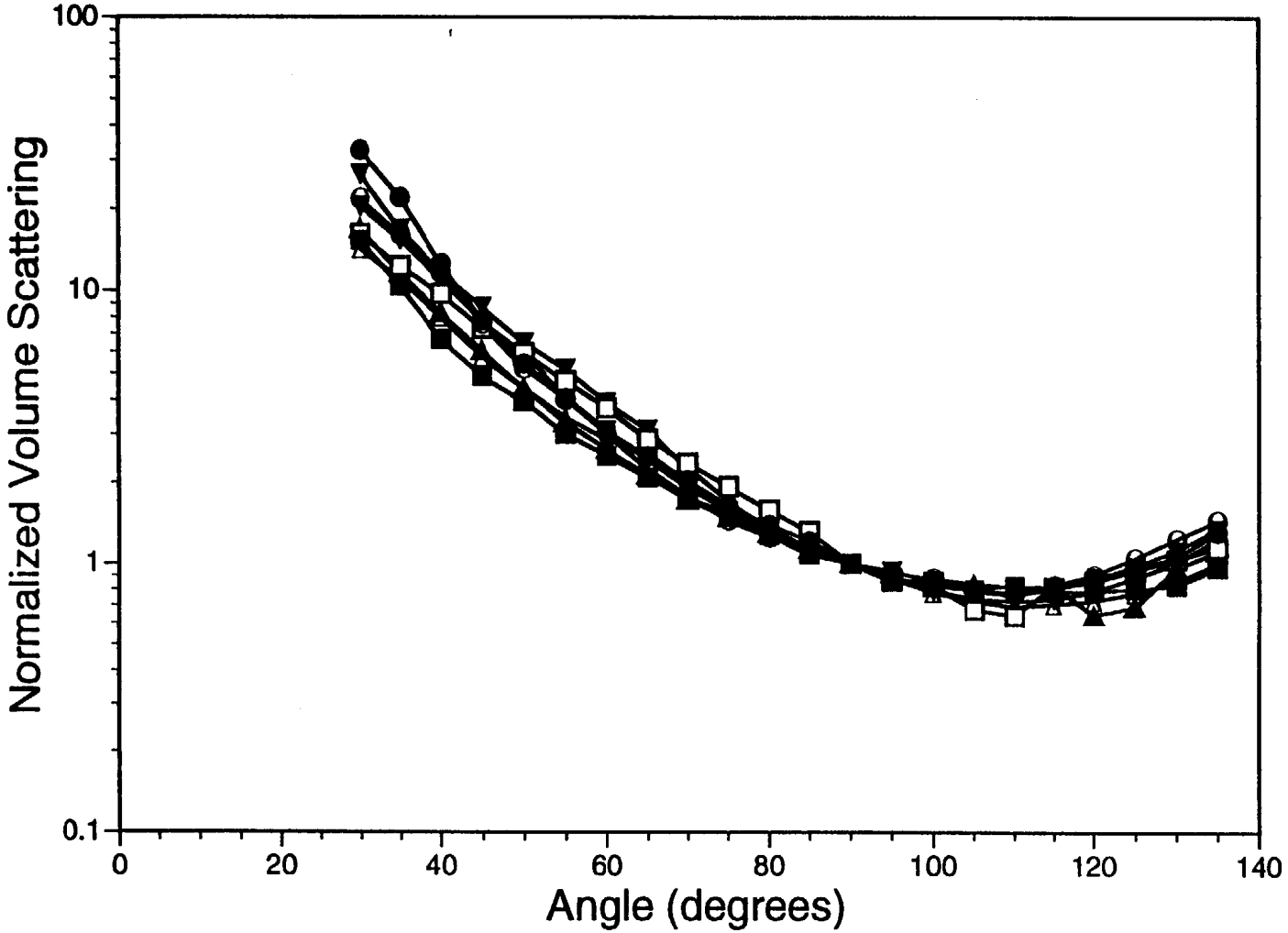
Normalized Volume Scattering
100
10
1
0.1
0
20
40
60
80
100
120
140
Angle (degrees)

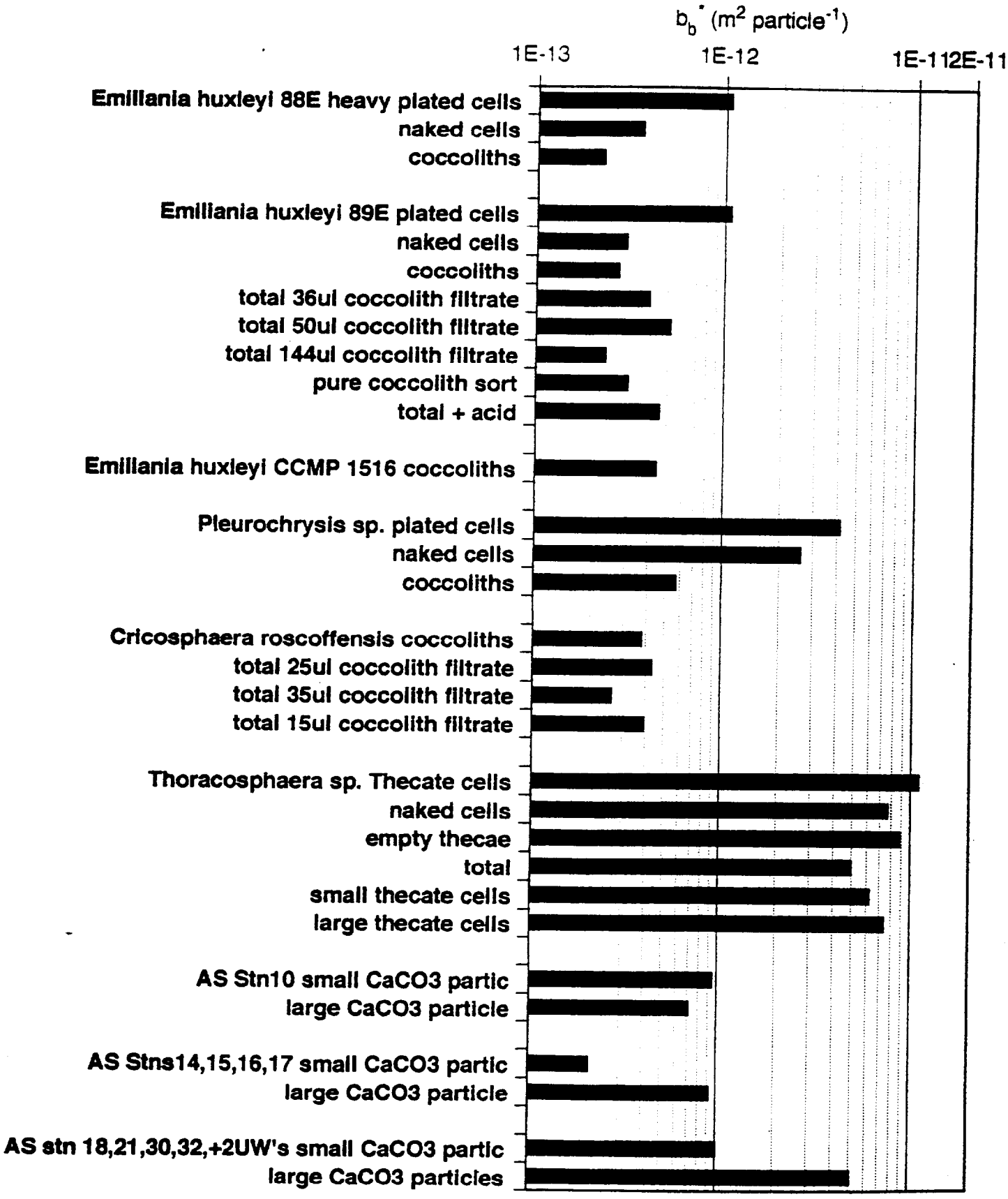
b_b^* (m^2 particle^{-1})
1E-13
1E-12
1E-11
2E-11
Emiliania huxleyi 88E heavy plated cells
naked cells
coccoliths
Emiliania huxleyi 89E plated cells
naked cells
coccoliths
total 36ul coccolith filtrate
total 50ul coccolith filtrate
total 144ul coccolith filtrate
pure coccolith sort
total + acid
Emiliania huxleyi CCMP 1516 coccoliths
Pleurochrysis sp. plated cells
naked cells
coccoliths
Cricosphaera roscoffensis coccoliths
total 25ul coccolith filtrate
total 35ul coccolith filtrate
total 15ul coccolith filtrate
Thoracosphaera sp. Thecate cells
naked cells
empty thecae
total
small thecate cells
large thecate cells
AS Stn10 small CaCO3 partic
large CaCO3 particle
AS Stns14,15,16,17 small CaCO3 partic
large CaCO3 particle
AS stn 18,21,30,32,+2UW's small CaCO3 partic
large CaCO3 particles

Fig 3

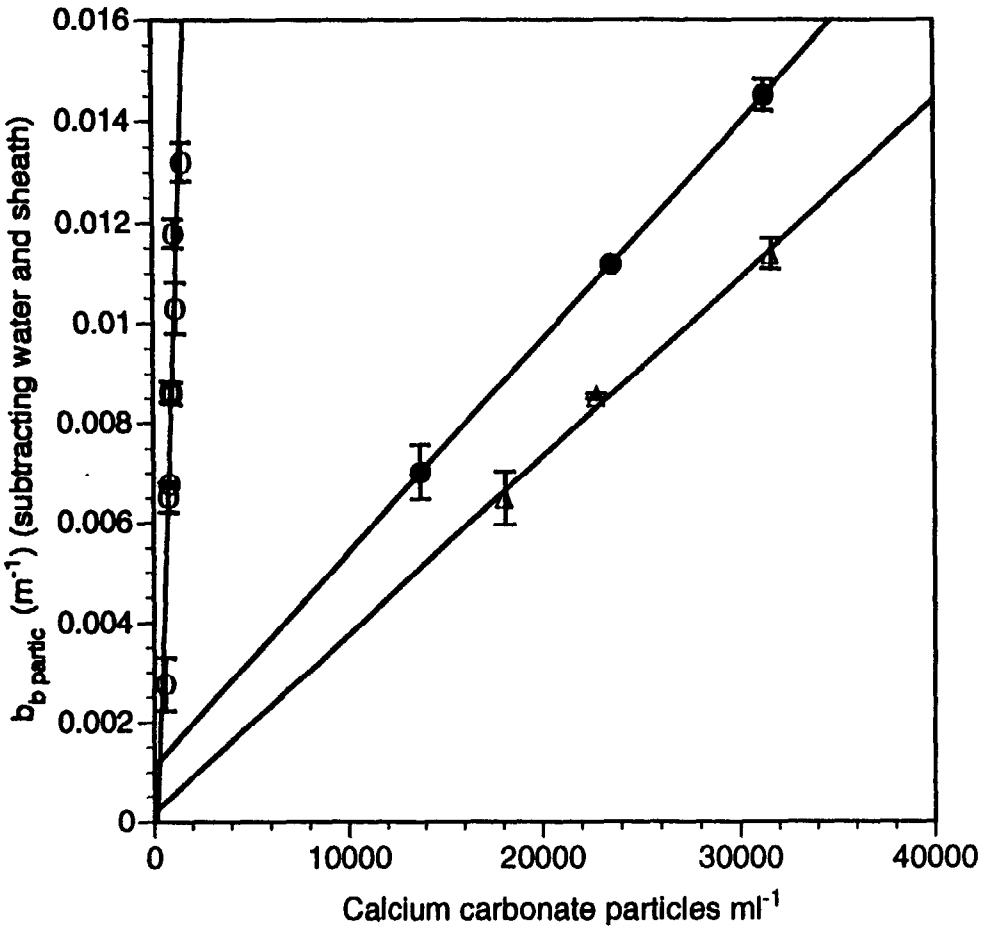
0.016
0.014
0.012
0.01
0.008
0.006
0.004
0.002
0
$b_{b\ partic}$ (m^{-1}) (subtracting water and sheath)
0
10000
20000
30000
40000
Calcium carbonate particles ml^{-1}

Fig 4

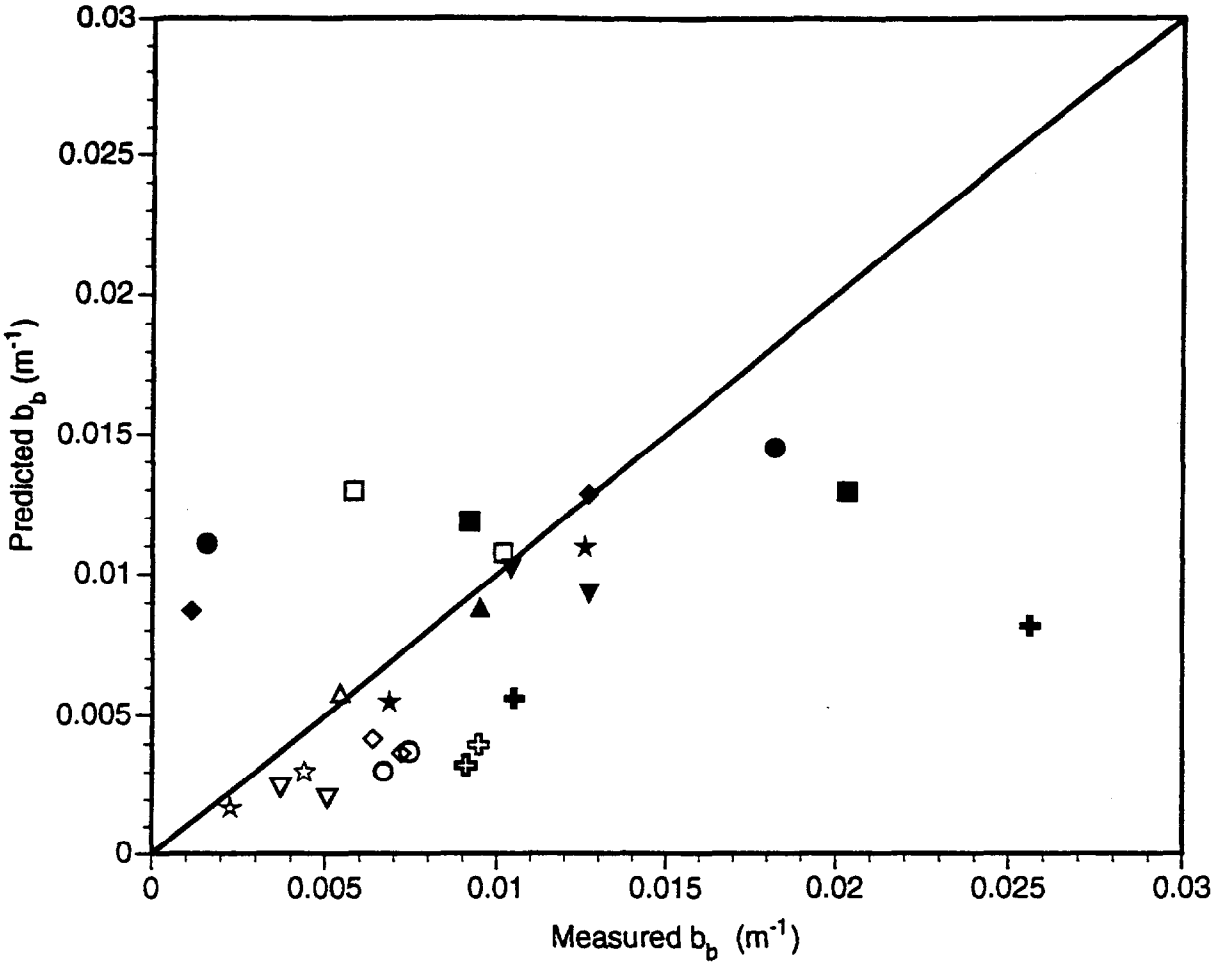
0.03
0.025
0.02
0.015
0.01
0.005
0
Predicted b_b (m^{-1})
0
0.005
0.01
0.015
0.02
0.025
0.03
Measured b_b (m^{-1})

Fig 5

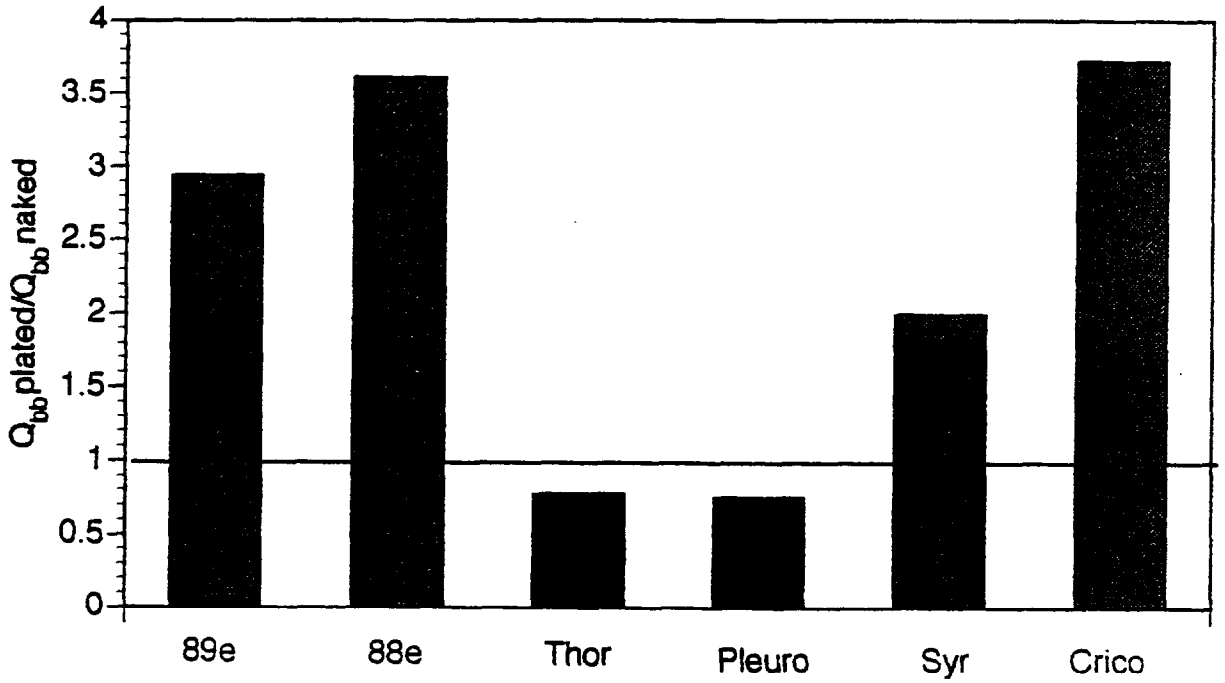
Q_{bb} plated/Q_{bb} naked
4
3.5
3
2.5
2
1.5
1
0.5
0
89e
88e
Thor
Pleuro
Syr
Crico

Fig 6

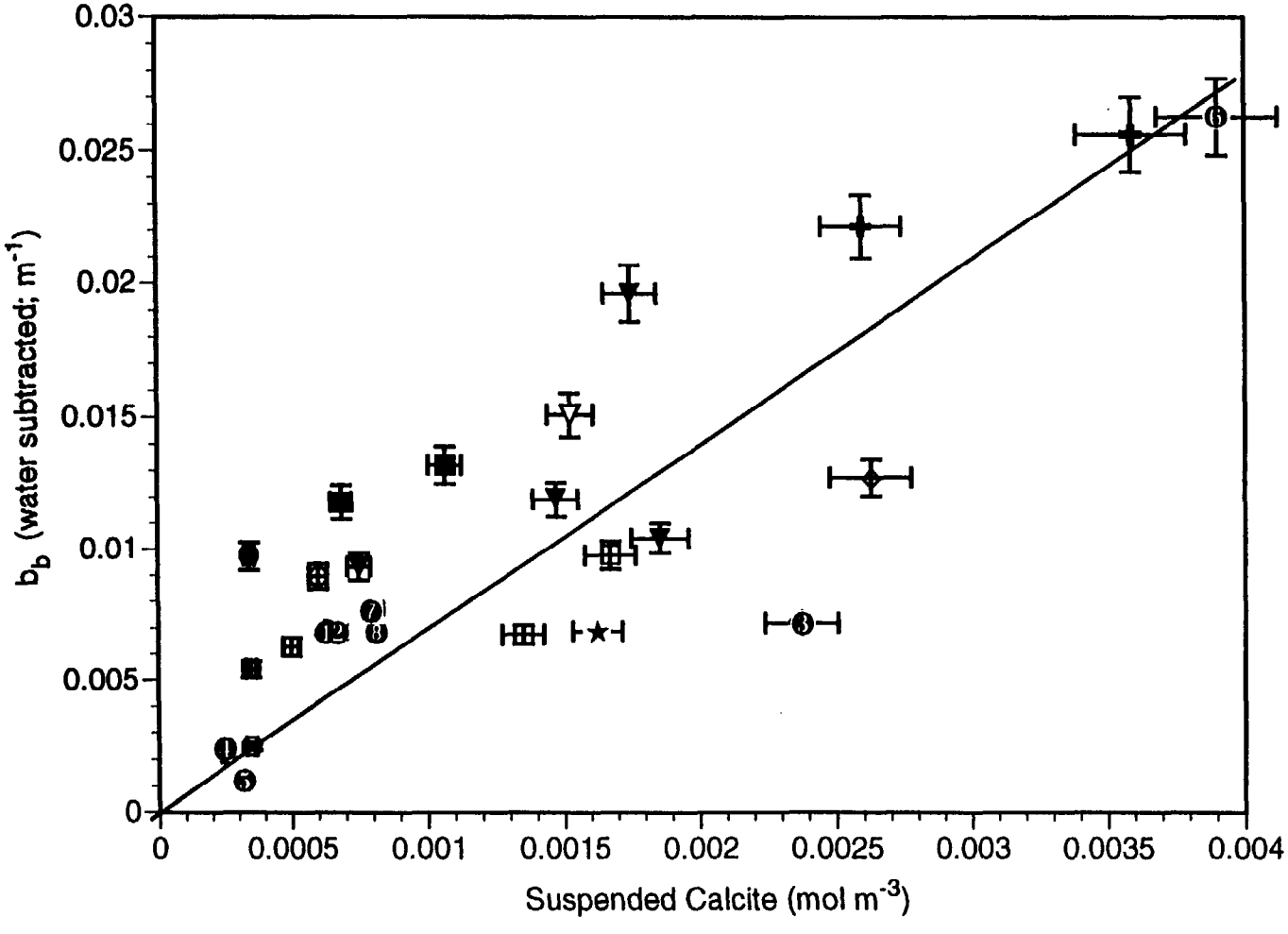
0.03
0.025
0.02
0.015
0.01
0.005
0
b_b (water subtracted; m^{-1})
0
0.0005
0.001
0.0015
0.002
0.0025
0.003
0.0035
0.004
Suspended Calcite (mol m^{-3})

Fig 7

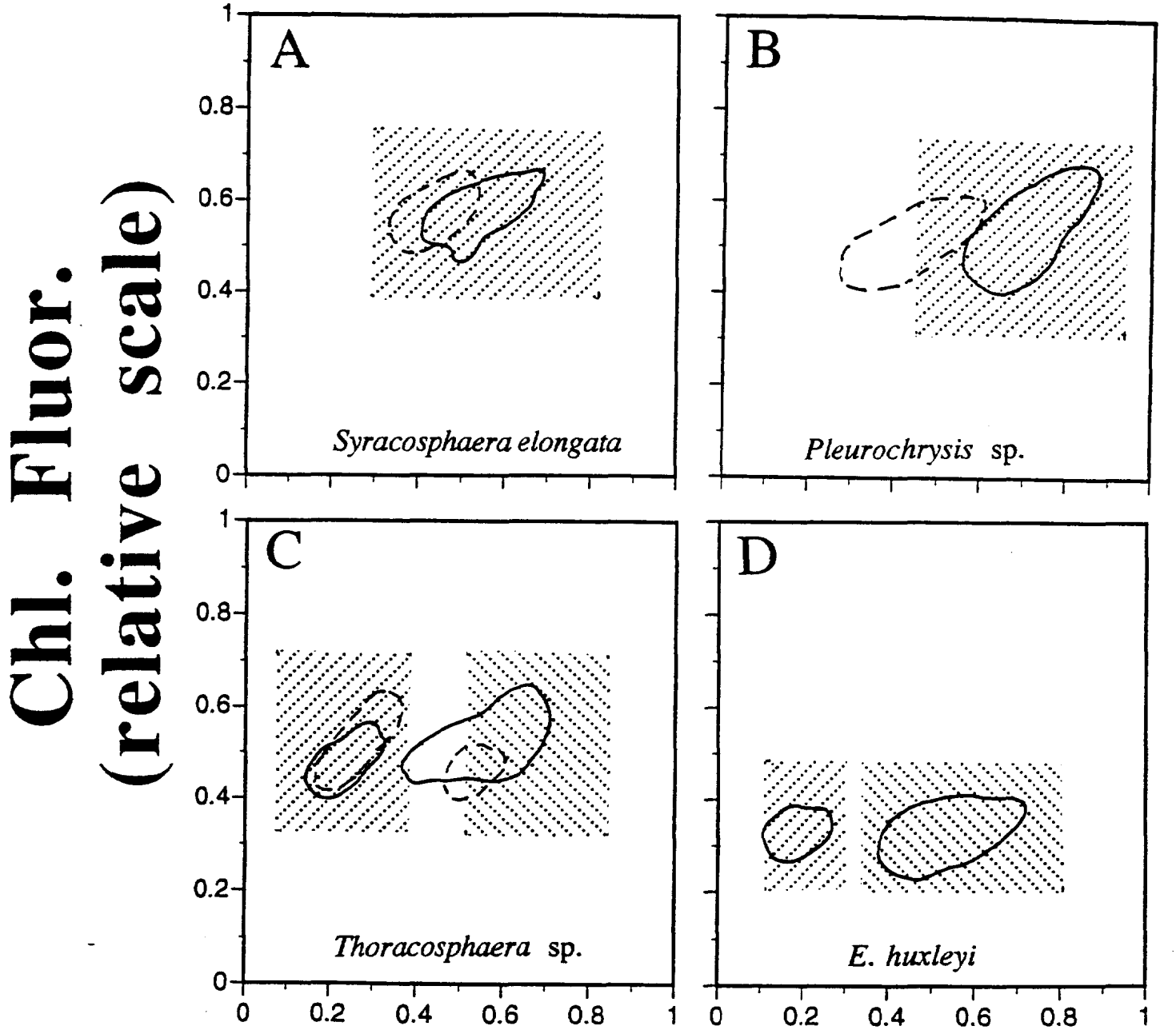
Chl. Fluor.
(relative scale)
A
B
C
D
Syracosphaera elongata
Pleurochrysis sp.
Thoracosphaera sp.
E. huxleyi
0
0.2
0.4
0.6
0.8
1
90° Vol. Scat.
(relative scale)

Fig 8

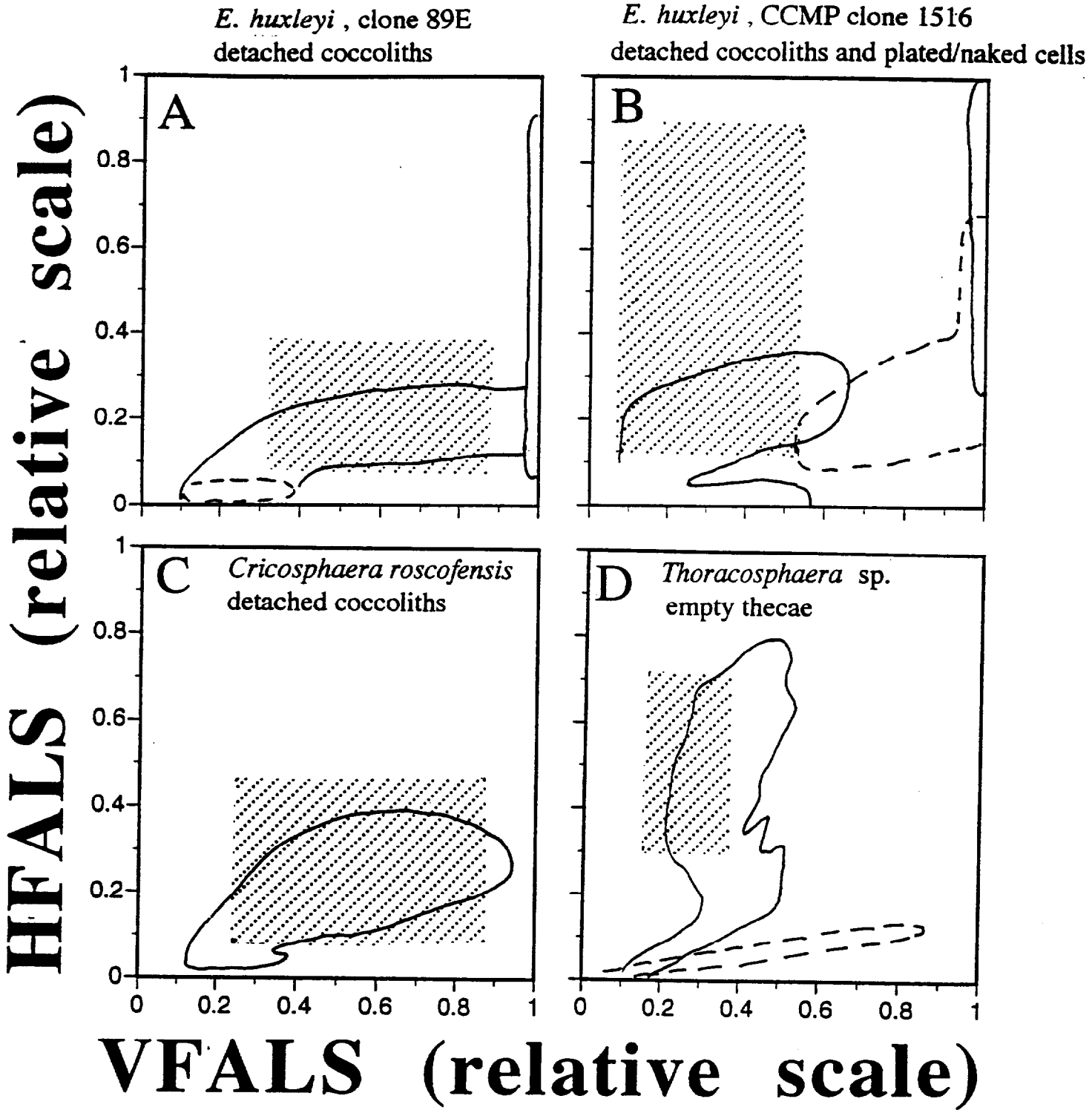
E. huxleyi , clone 89E
detached coccoliths
E. huxleyi , CCMP clone 1516
detached coccoliths and plated/naked cells
A
B
C
Cricosphaera roscofensis
detached coccoliths
D
Thoracosphaera sp.
empty thecae
HFALS (relative scale)
VFALS (relative scale)
0
0.2
0.4
0.6
0.8
1

Fig 9

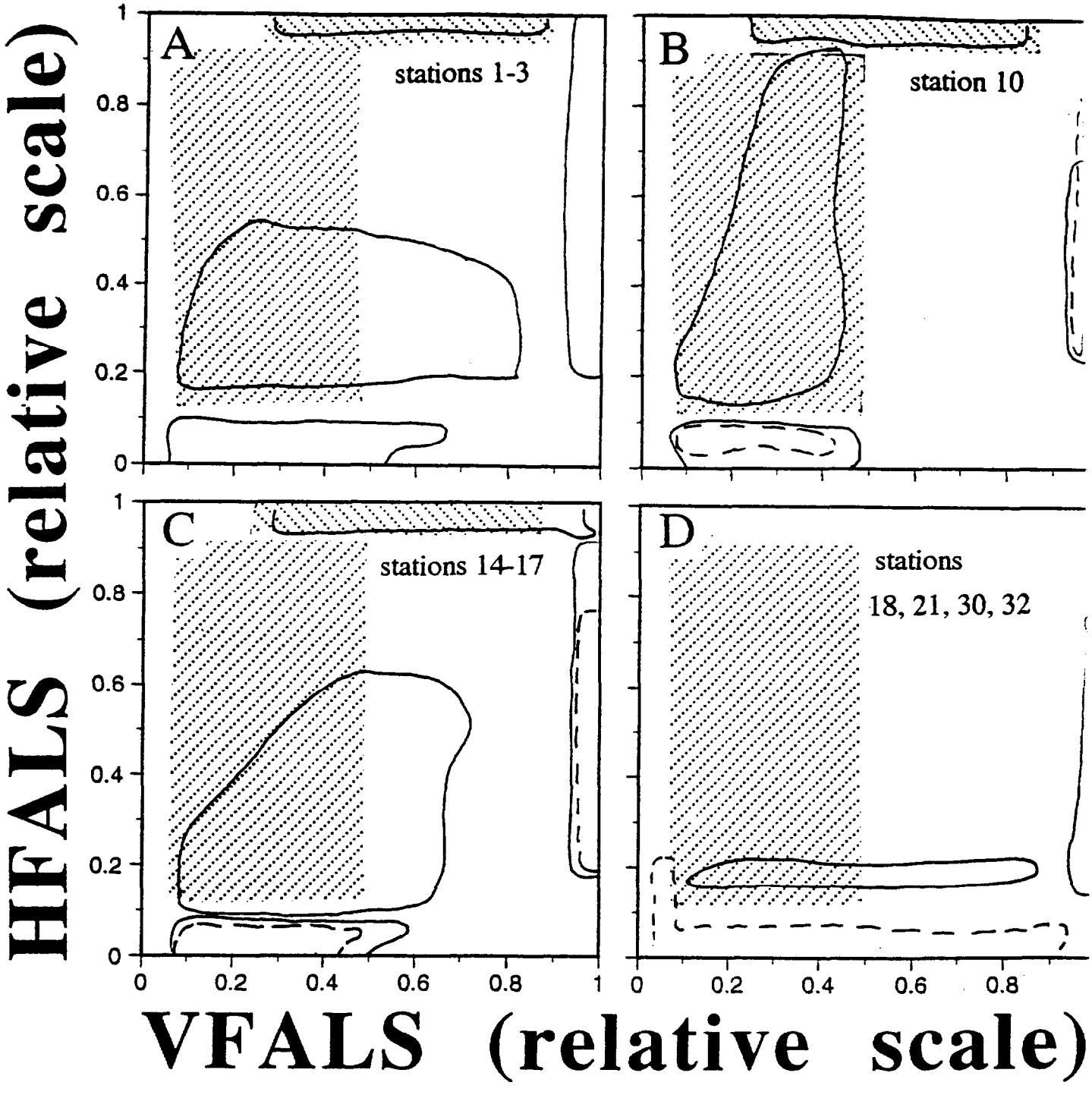
A
stations 1-3
B
station 10
C
stations 14-17
D
stations
18, 21, 30, 32
HFALS (relative scale)
VFALS (relative scale)
0
0.2
0.4
0.6
0.8
1

Fig 10

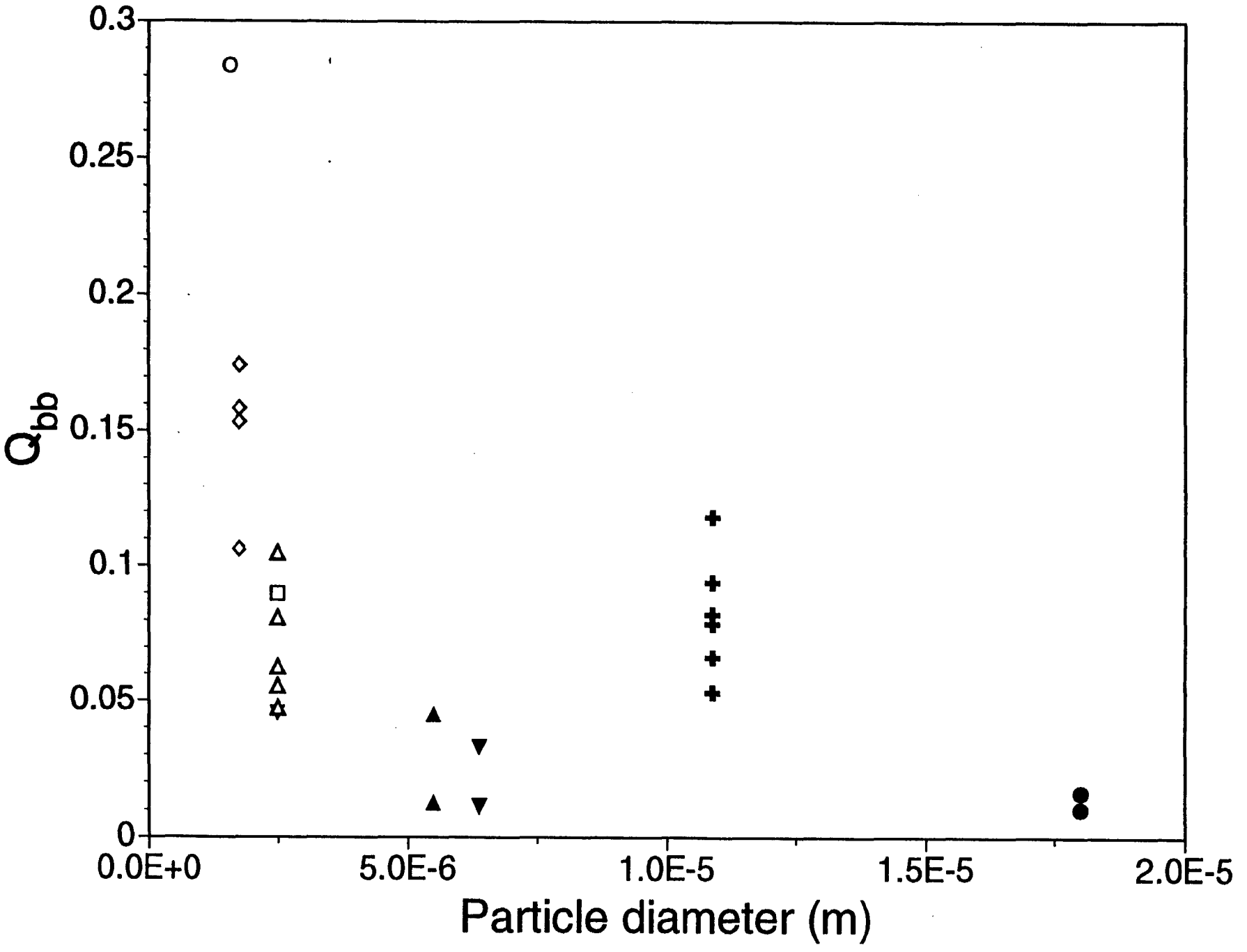
0.3
0.25
0.2
0.15
0.1
0.05
0
Q_{bb}
0.0E+0
5.0E-6
1.0E-5
1.5E-5
2.0E-5
Particle diameter (m)

Fig 11

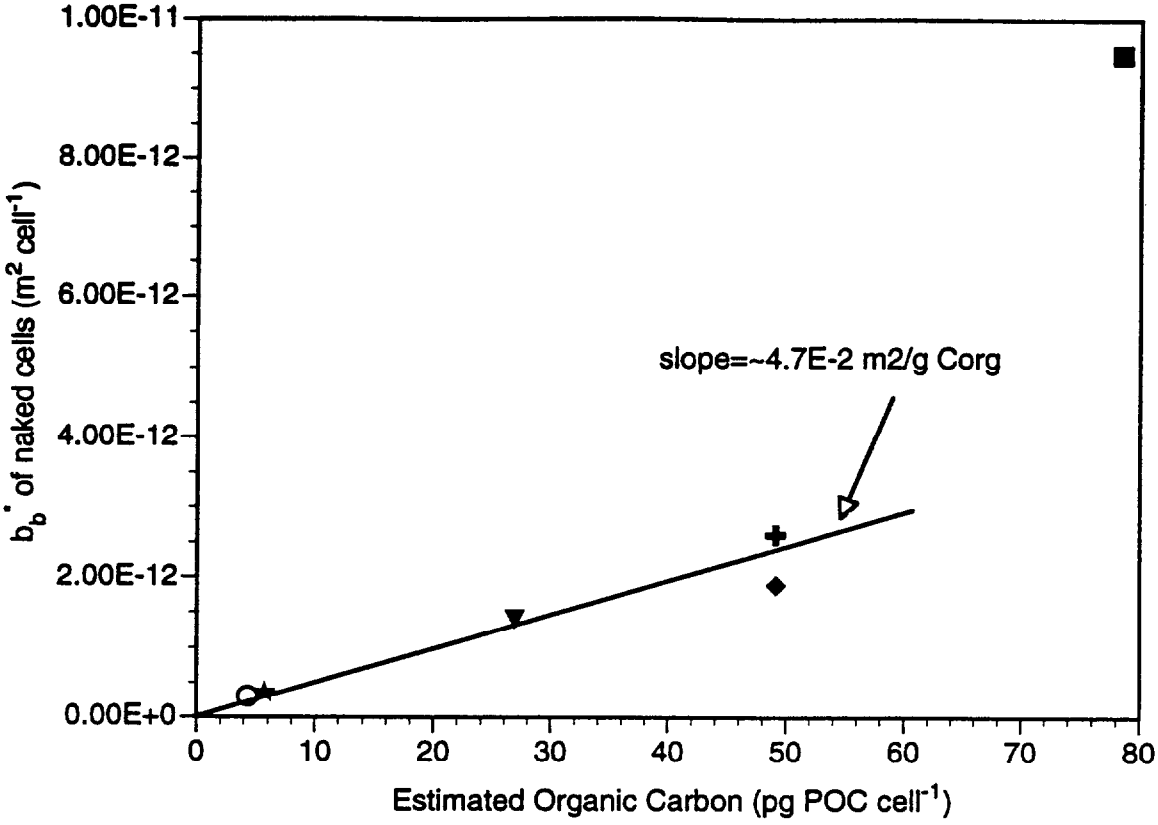
1.00E-11
8.00E-12
6.00E-12
4.00E-12
2.00E-12
0.00E+0
b_b^* of naked cells (m^2 $cell^{-1}$)
slope=~4.7E-2 m2/g Corg
0
10
20
30
40
50
60
70
80
Estimated Organic Carbon (pg POC $cell^{-1}$)

Fig 12

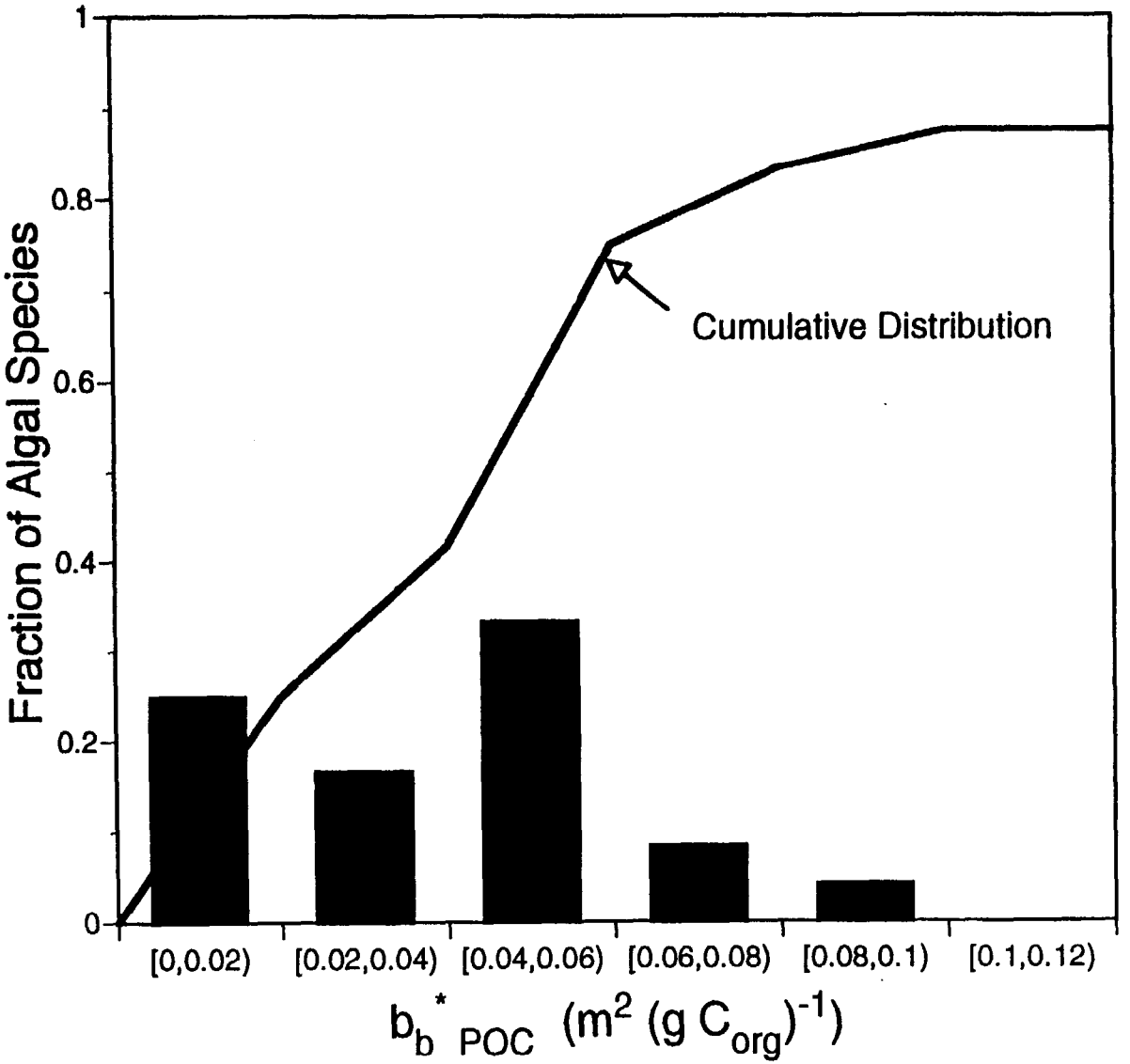
1
0.8
0.6
0.4
0.2
0
Fraction of Algal Species
Cumulative Distribution
[0,0.02)
[0.02,0.04)
[0.04,0.06)
[0.06,0.08)
[0.08,0.1)
[0.1,0.12)
b_b^* POC (m^2 (g C_{org})$^{-1}$)

Fig 13

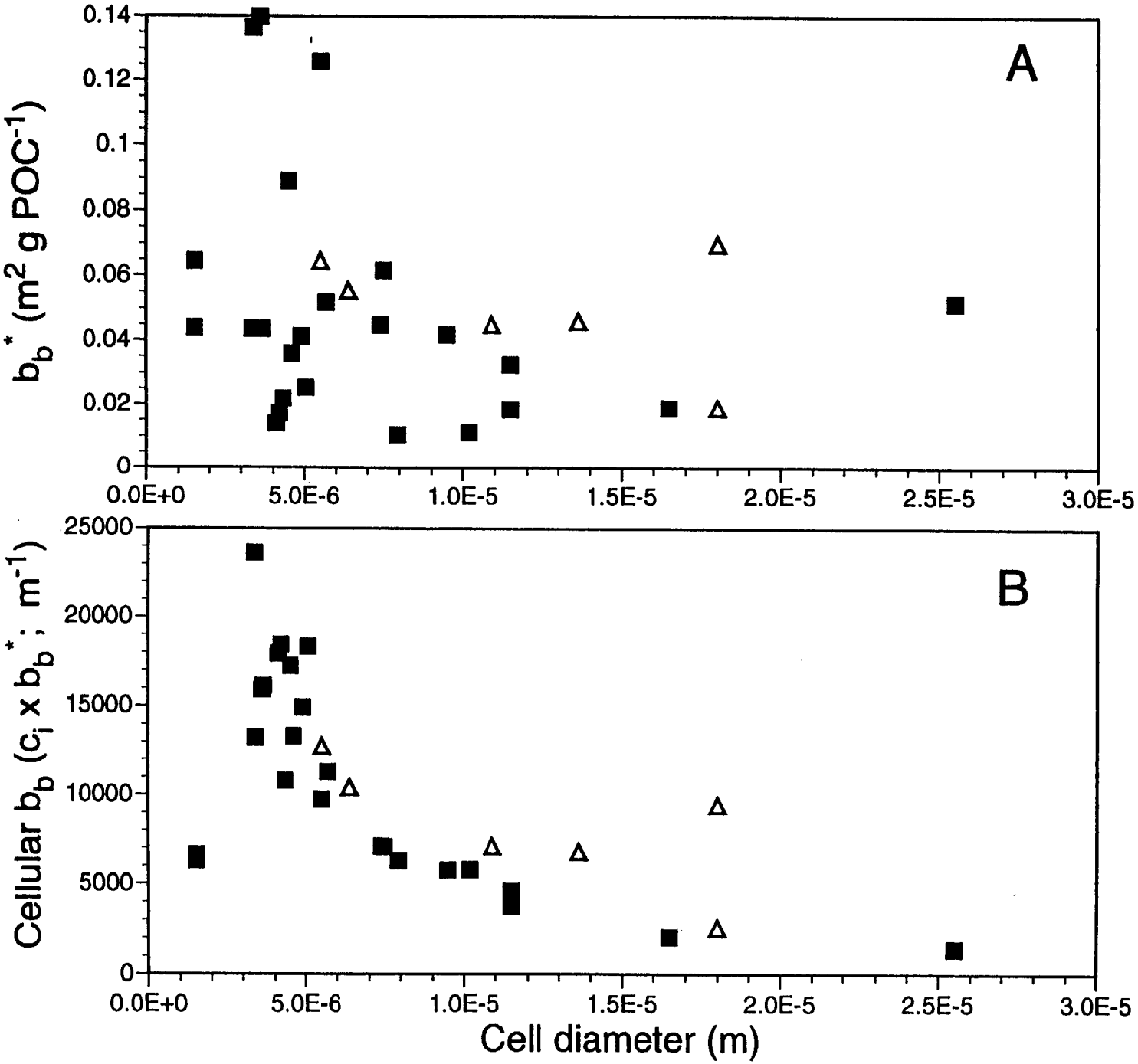
A
B
b_b^* (m^2 g POC^{-1})
Cellular b_b (c_i x b_b^*; m^{-1})
Cell diameter (m)
0.14
0.12
0.1
0.08
0.06
0.04
0.02
0
25000
20000
15000
10000
5000
0.0E+0
5.0E-6
1.0E-5
1.5E-5
2.0E-5
2.5E-5
3.0E-5

Fig 14